CHAPTER IV

RESULTS AND DISCUSSION

In this chapter, the experimental results and discussion are described in three main parts. In the first part, the preparation of pure and V-doped TiO_2 photocatalysts is discussed. In the second part, the coating of TiO_2 sol on the substrates is presented. Finally, the photocatalytic efficiency determination of the synthesized TiO_2, as well as commercial P-25 are analyzed and discussed.

4.1 Preparation of TiO_2 photocatalysts

4.1.1 Pure TiO_2

A. Using HCl acid as a hydrolysis catalyst (Sol 1)

The formation of titanium dioxide sol was based on the hydrolysis of Ti butoxide in the presence of HCl catalyst. The precursor solutions of various compositions (shown in Table 3.1) were aged at room temperature for 50 days. Figure 4.1 illustrates the appearance of the TiO_2 sols obtained from these precursors. By visual observation over the aging time span of 50 days, several trends for the sol formation were drawn. Firstly, by comparison of series A, B and C (increasing amount of HCl), the sol formation as visually seen by the milky appearance took place in series C followed by series B and A, respectively. This observation indicated that the sol formation was accelerated by the HCl catalyst. Secondly, by comparison of series A and E (increasing amount of H_2O), the sol formation in series E was faster than series A, indicating that the hydrolysis and therefore sol formation was dependent on the amount of water. In the case of series D, which had high amounts of both HCl and H_2O, the hydrolysis was very fast and the white precipitate occurred in a few days. The TiO_2 precipitate was a large agglomerate of the finer particles.

From the above results, the sol formation was found to be largely dependent on the amount of HCl and H_2O. It was accelerated by the addition of H_2O and HCl catalyst. When the quantity of H_2O and HCl addition was excessive, fast hydrolysis occurred and fast precipitation took place. This kind of product was defied as an unstable sol. Slow hydrolysis and stable sol was undertaken by adding a small amount of H_2O and HCl, resulting in very small size TiO_2 particles. In the case of the TiO_2 sol obtained from Sol_1A and Sol_1E, the hydrolysis rate seemed to be slow enough to get the stable sol in comparison with Sol_1B, Sol_1C and Sol_1D.

Finally, the difference in concentration of the Ti precursor also played an important role. Higher concentration of $Ti(OBu)_4$ resulted in faster sol formation and greater yield. For example, Sol_1Aa (0.07 M $Ti(OBu)_4$) gave much smaller content of TiO_2 particles than Sol_1Ae (0.7 M $Ti(OBu)_4$). However, high concentrated $Ti(OBu)_4$ precursor resulted in the precipitate, instead of the stable sol. Table 4.1 summarizes the results of visual observation during the entire course of sol preparation. The letters TP, TC, M and P denote transparent, translucent, milky, and precipitating appearances, respectively.

It is important to point out again that the stability of the TiO_2 sol depended on concentration of the $Ti(OBu)_4$, as well as the amount of H_2O, and HCl. To obtained stable sols, the amounts of these starting reagents must be well manipulated to obtain the optimum condition to synthesize the TiO_2 sol for further photocatalyst application. Here, the TiO_2 sols obtained from precursors Sol_1Ad and Sol_1Ed were found to have suitable stability since these sols did not undergo bulk precipitation after aging for several weeks.

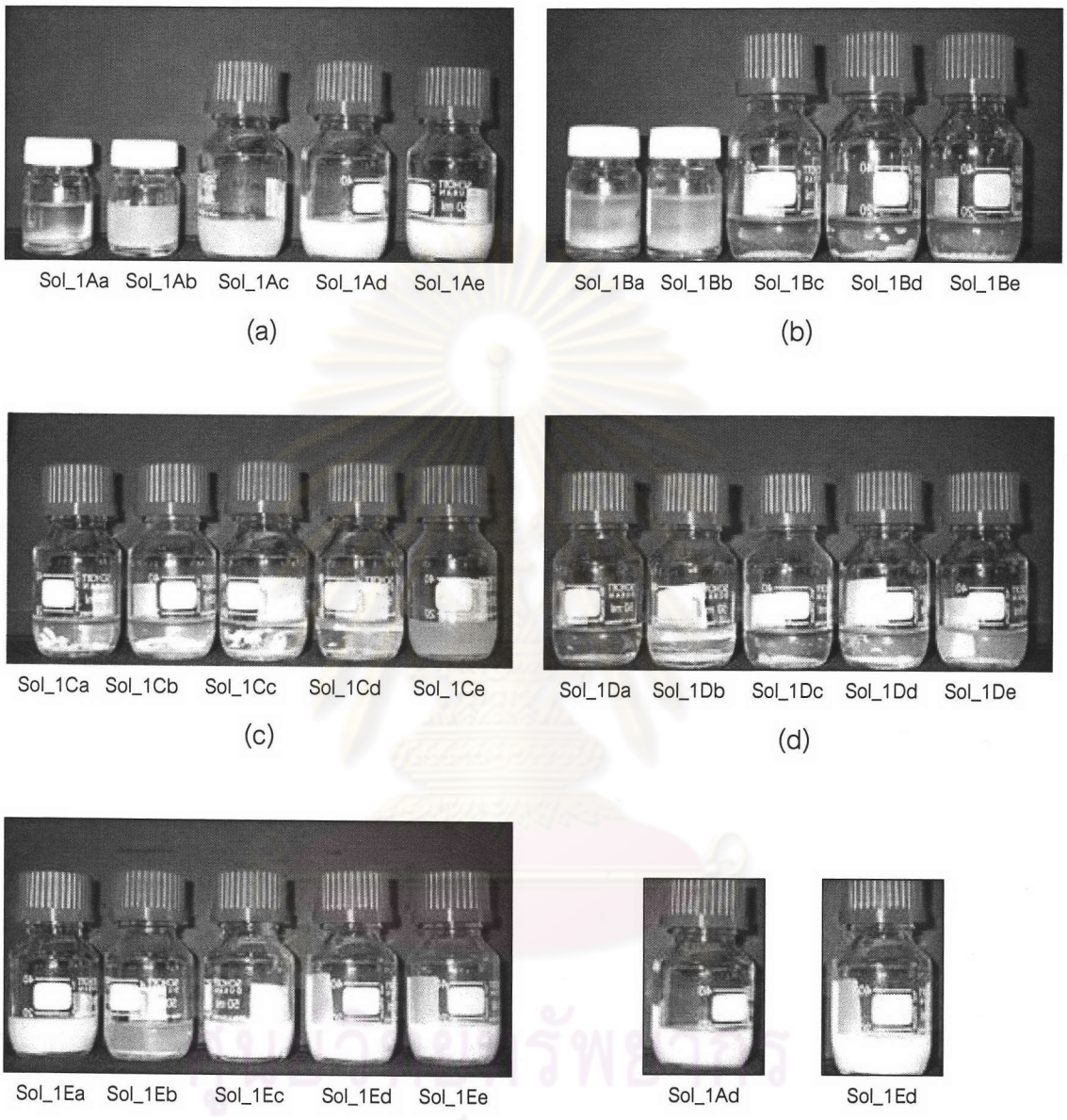

Figure 4.1 Photographs of the sols obtained by aging the Ti precursors of various compositions for 50 days (using HCl catalyst)

Table 4.1 Visual observation of Sol_1 aged for 50 days

Samples code	Concentration of $Ti(OBu)_4$ (Molar)	H_2O: EtOH: HCl (Volume ratio)	Visual observation
Sol_1Aa	0.07		TP + P
Sol_1Ab	0.20		TC + P
Sol_1Ac	0.30	1:3:1	TC + PP
Sol_1Ad	0.50		M
Sol_1Ae	0.70		M + P
Sol_1Ba	0.07		TC + P
Sol_1Bb	0.20		TC + P
Sol_1Bc	0.30	1:2:2	TP + P
Sol_1Bd	0.50		TP+ PP
Sol_1Be	0.70		TP + PP
Sol_1Ca	0.07		TP + PPP
Sol_1Cb	0.20		TP + PPP
Sol_1Cc	0.30	1:1:3	TP + PPP
Sol_1Cd	0.50		TP + PPP
Sol_1Ce	0.70		TC + P
Sol_1Da	0.07		TP + PP
Sol_1Db	0.20		TP + PP
Sol_1Dc	0.30	1.5:1.5:2	TP + PP
Sol_1Dd	0.50		TP + PP
Sol_1De	0.70		TP + PP
Sol_1Ea	0.07		M + P
Sol_1Eb	0.20		TC + P
Sol_1Ec	0.30	2:2:1	M + PP
Sol_1Ed	0.50		M
Sol_1Ee	0.70		M + PP

TP: transparent, TC: translucent, M: milky, and P: precipitated

Figure 4.2 shows the XRD patterns of dried TiO_2 powders obtained from Sol_1Ad (0.5 M, H_2O: EtOH: HCl = 1:3:1) prepared at room temperature at different aging times (10, 20, 30, 40 and 50 days). The letters A and R in the XRD patterns mark the diffraction peaks corresponded to anatase and rutile phases, respectively. The major peak corresponding to anatase phase appeared at 2θ = 25.3°, while that of the rutile phase appeared at 2θ = 27.5°. The XRD patterns indicated that all of the as-synthesized samples consisted of both anatase and rutile phases. Broad and low-intensity peaks of all samples indicated that the anatase and rutile phase had very fine crystallite size, and may also contain an amorphous along with crystalline TiO_2 phase. The TEM results (Figure 4.4) also support the XRD analysis that the as-synthesized sample consisted of very fine crystals together with an amorphous phase of either the titanium oxide or organic residue. Note that the average crystal size measured directly from TEM image was 3.0 nm which was slightly finer than the size calculated from XRD peaks. In addition, the anatase and rutile crystals are not clearly identified in this TEM image. The presence of amorphous phase is common for oxide ceramics prepared by wet-chemical process. For example, Douglas and Merrilea also found that the TiO_2 samples produced via sol-gel method also consisted of amorphous structure [55]. Comparing diffractions (a) to (e), the relative intensity of the peaks corresponding to rutile increased with increasing aging time, indicating anatase-to-rutile phase transformation occurring in the suspension. Almost anatase phase transformed to rutile phase at 50 days of aging time. Moreover, it was anticipated that rutile phase had better crystallinity and larger crystallite size since the peaks became sharper. It had been reported that anatase was the thermodynamically metastable phase while rutile was a most stable phase. Generally, the thermodynamically metastable anatase phase transformed to stable rutile phase [27].

Figure 4.3 shows the XRD patterns of as-synthesized TiO_2 powders obtained from Sol_1Ed (0.5 M $Ti(OBu)_4$), H_2O: EtOH: HCl = 2:2:1) at different aging times (10-50 days) prepared at room temperature. The phase compositions observed by XRD were also the mixture of anatase and rutile phases, similar to Sol_1Ad. For the TiO_2 samples aged for 10 days, the majority phase was anatase and the minority phase was rutile. The amorphous

phase was also observed along with the crystalline anatase and rutile phase. Similarly, it was observed that the anatase-rutile phase transformation was promoted by prolonged aging. The rutile phase gradually increased from 35% (10 days) to 70% with the 30 days of aging time. The complete transformation to rutile was found at 40 days of aging time (Figure 4.3(d)). Narrower and higher intensity peaks of samples obtained from Sol_1Ed with 40 and 50 days of aging time (Figure 4.3 (d, e)) indicate that both samples were made of relative large crystallites. However, the prolonged aging time not only altered the phase transformation but also influenced the crystallite size of TiO_2. It resulted in the crystallite growth of both anatase and rutile, as reflected by the sharpen XRD peaks corresponding to rutile phase in Figure 4.3 (d) compared to those of anatase and rutile phases in Figure 4.2 (d). The XRD result was consistent with the result from TEM observation as shown in Figure 4.5 (Sol_1Ed aged for 40 days). Irregular shape of pure rutile crystal of average size 10 nm-wide and 60 nm-long was clearly seen. The phase composition and the crystallite size of all samples derived from XRD pattern obtained from Sol_1 are listed in Table 4.2.

It is important to note that although the as-synthesized TiO_2 obtained from Sol_1Ad and Sol_1Ed (Figure 4.6 (a and b)) show small nanocrystallite size, they exist in the form of large aggregated nanoparticles (average size around 700-1,200 nm or 0.7-1.2 μm). The size and microstructure of calcined powders obtained form Sol_1 are shown in Figure 4.7 and 4.8, respectively.

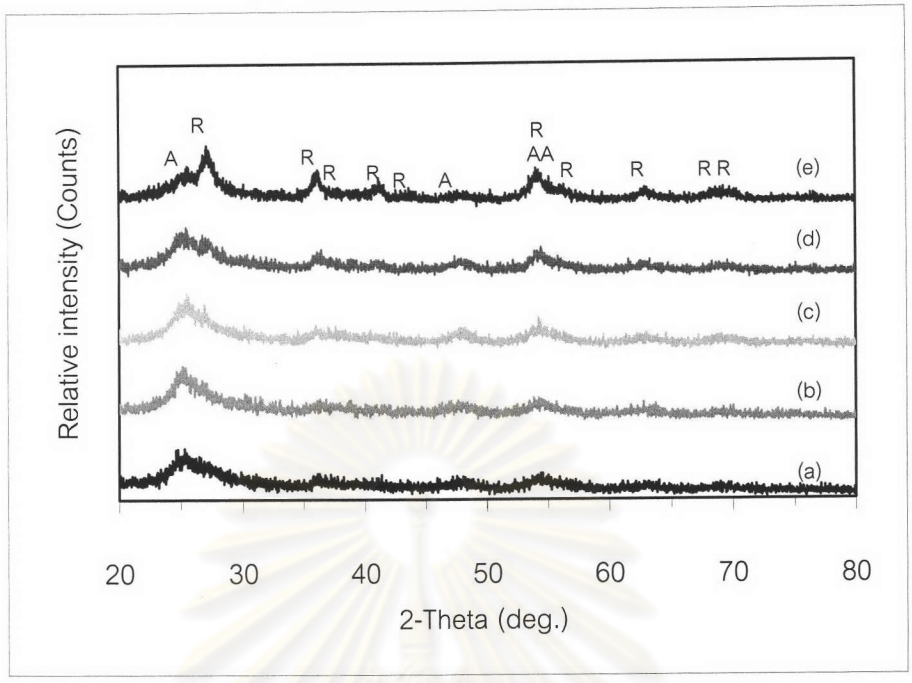

Figure 4.2 XRD patterns of the as-synthesized powders obtained from Sol_1Ad (H_2O: EtOH: HCl = 1:3:1) aged for; (a) 10 days, (b) 20 days, (c) 30 days, (d) 40 days, and (e) 50 days; A = Anatase, R = Rutile

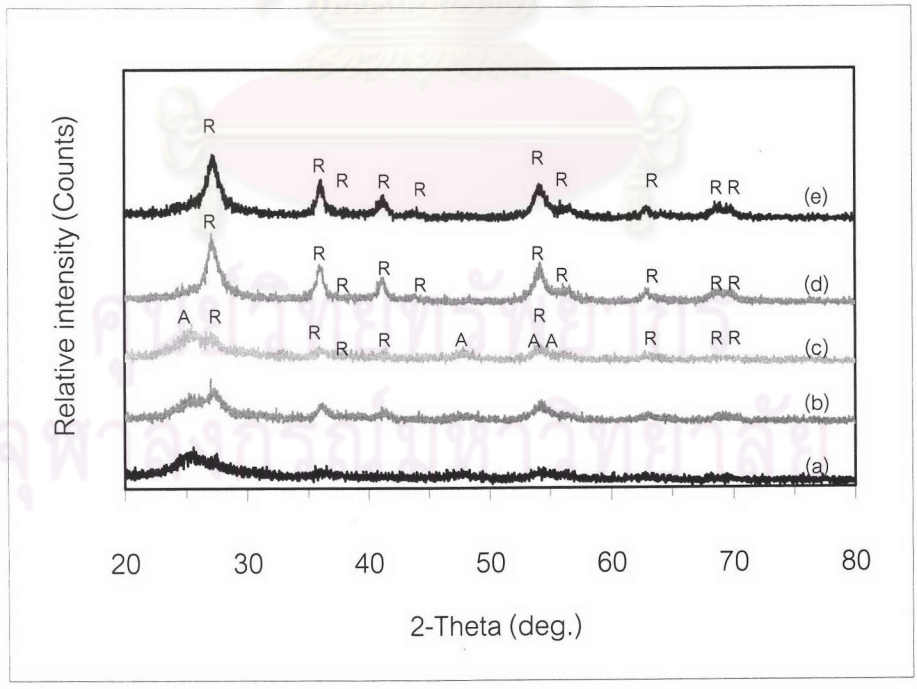

Figure 4.3 XRD patterns of the as-synthesized powders obtained from Sol_1Ed (H_2O: EtOH: HCl = 2:2:1) aged for (a) 10 days, (b) 20 days, (c) 30 days, (d) 40 days, and (e) 50 days; A = Anatase, R = Rutile

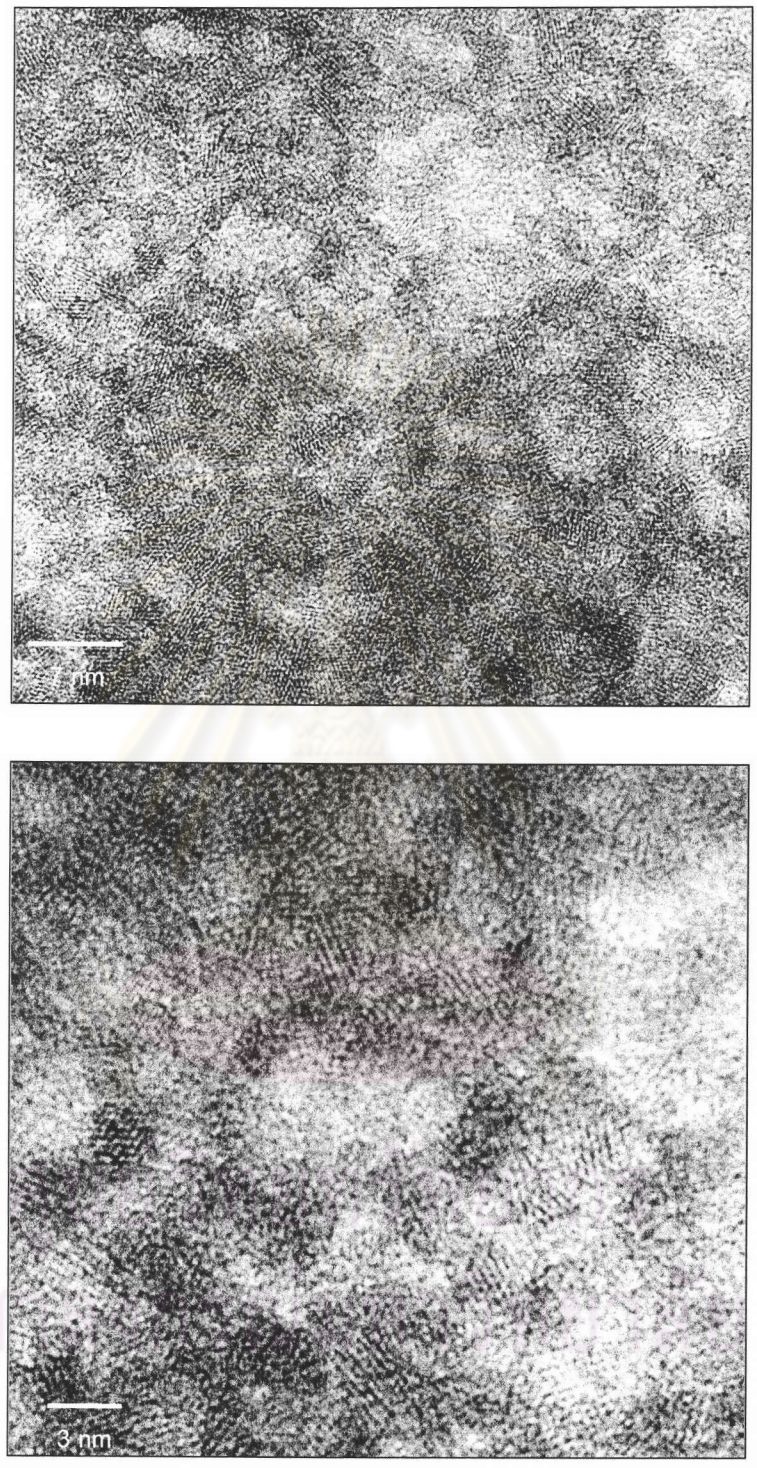

Figure 4.4 TEM images of as-synthesized TiO_2 powders obtained from Sol_1Ad (H_2O:EtOH:HCl = 1:3:1) aged for 40 days

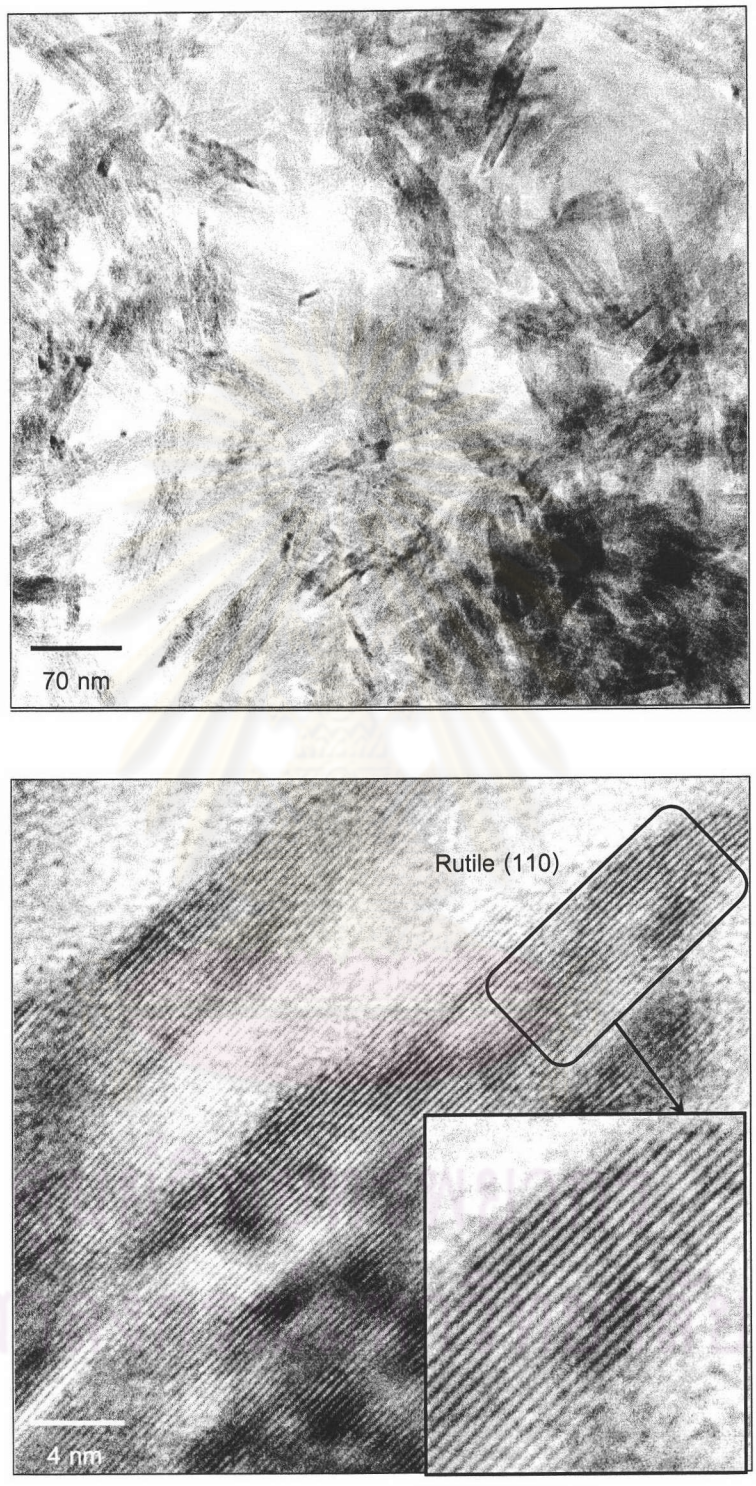

Figure 4.5 TEM images of as-synthesized TiO_2 powders obtained from Sol_1Ed (H_2O:EtOH:HCl = 2:2:1) aged for 40 days (Inset shows d-spacing of 3.13 Å corresponding to (110) plane of rutile)

Table 4.2 Phase composition and crystallite size of the pure TiO_2 powders (uncacined) obtained from Sol_1Ad and Sol_1Ed

Samples code	Phase composition (A: R)	Crystallite size[a] (nm.)	
		d_A	d_R
Sol_1Ad_10days	70:30	3.8	4.2
Sol_1Ad_20days	65:35	3.4	4.7
Sol_1Ad_30days	60:40	4.1	7.2
Sol_1Ad_40days	55:45	4.9	7.7
Sol_1Ad_50days	35:65	6.4	7.3
Sol_1Ed_10days	65:35	3.3	4.3
Sol_1Ed_20days	35:65	4.1	3.6
Sol_1Ed_30days	30:70	5.3	7.8
Sol_1Ed_40days	0:100	-	9.1
Sol_1Ed_50days	0:100	-	9.6

a = calculated from XRD peaks

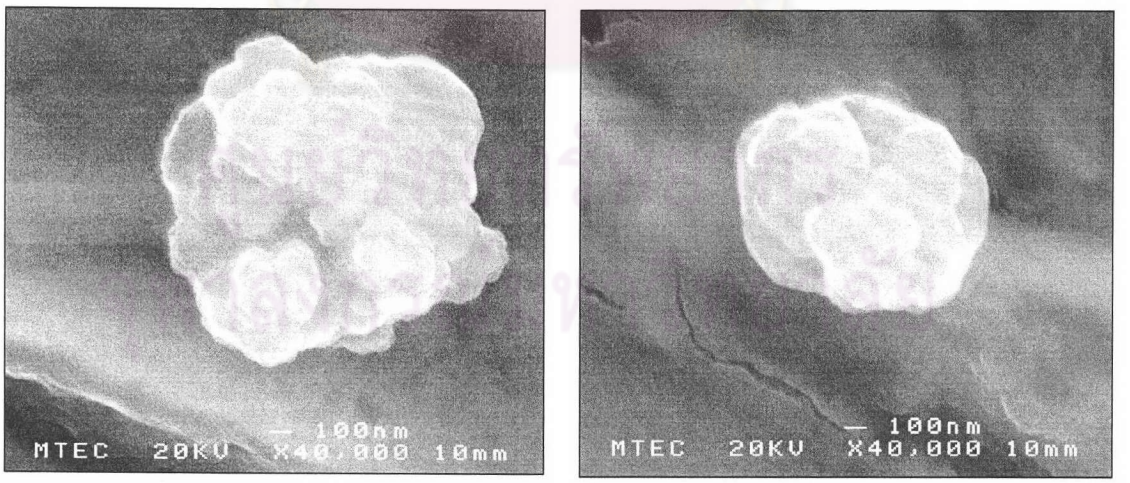

(a) (b)

Figure 4.6 SEM images of as-synthesized TiO_2 powders obtained from (a) Sol_1Ad (1:3:1) and (b) Sol_1Ed (2:2:1) aged for 40 days

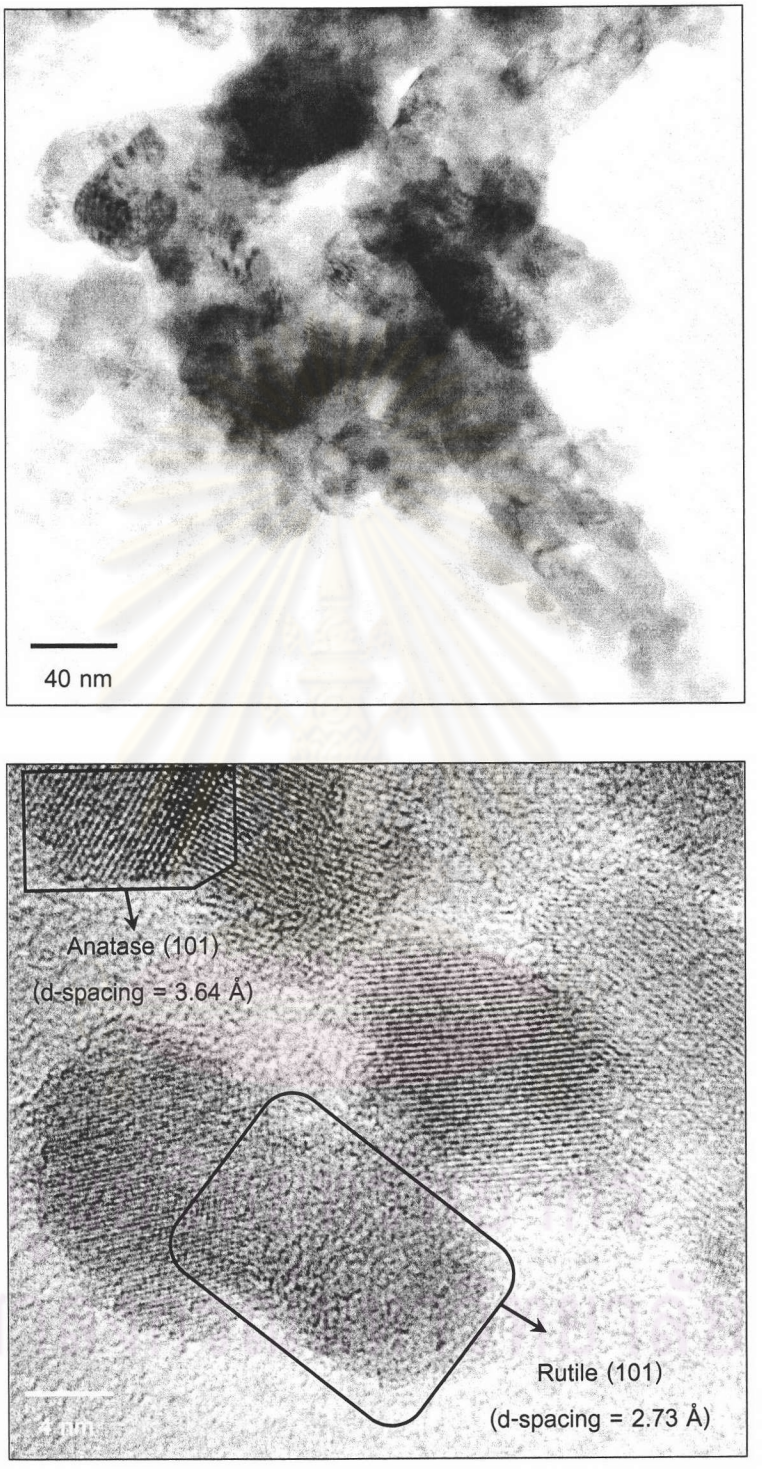

Figure 4.7 TEM images of TiO_2 powders obtained from Sol_1Ad (H_2O: EtOH: HCl = 1:3:1) aged for 40 days and calcined at 400°C for 4h

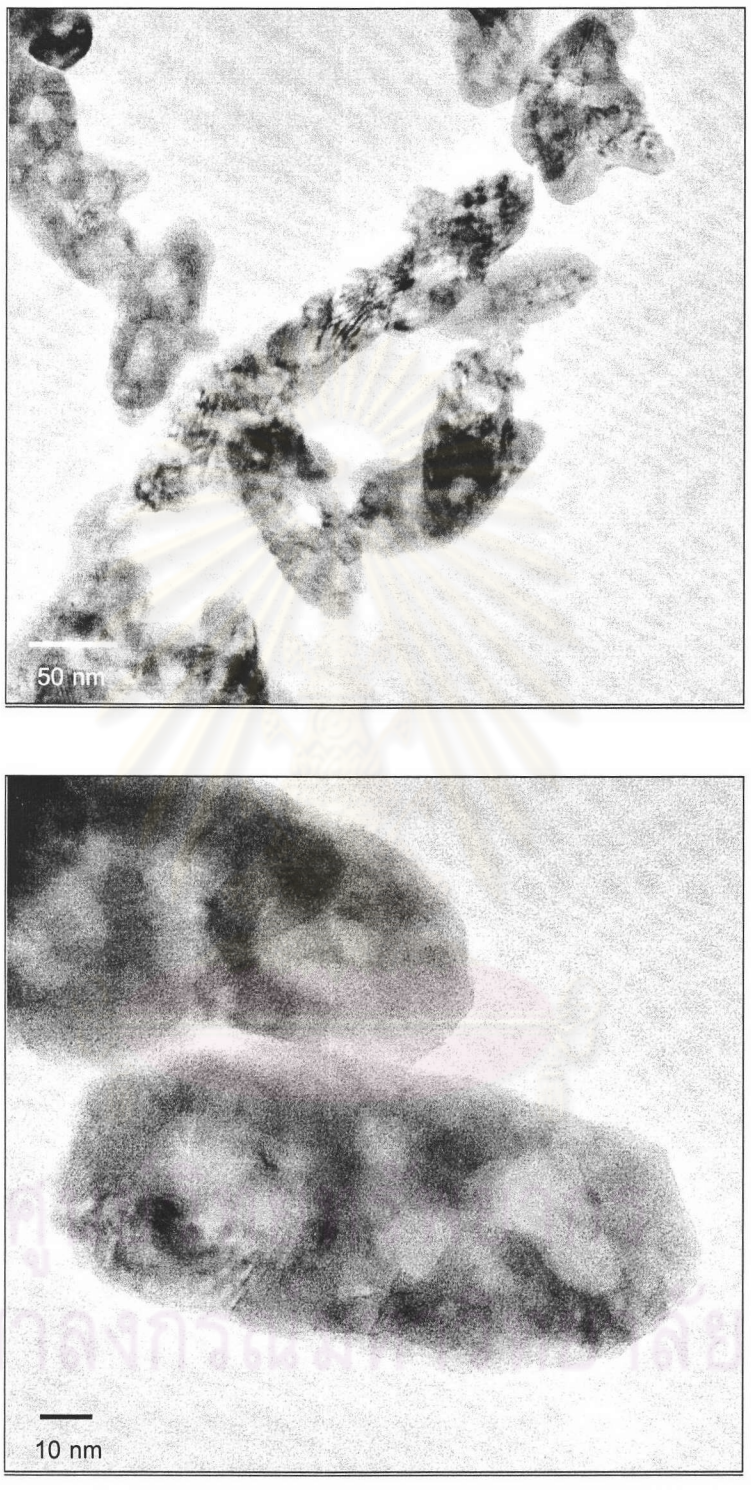

Figure 4.8 TEM images of the "rutile" crystal (59 nm wide x 134 nm long) obtained from Sol_1Ed (H_2O: EtOH: HCl = 2:2:1) aged for 40 days and calcined at 400°C for 4h

B. Using HNO_3 as a hydrolysis catalyst (Sol_2)

In order to further investigate the effect of the type of acidic catalyst on the phase formation of the TiO_2, the HNO_3 was chosen as the alternative to the HCl catalyst. Figure 4.9 is XRD patterns of the as-synthesized samples (series "Sol_2") obtained from the precursors of the same Ti concentration but containing different amounts of HNO_3 catalyst aged for 20 days. According to the XRD pattern, the as-prepared sample obtained from Sol_2A (H_2O: EtOH: HNO_3 = 10:10:2) consisted of anatase as a major phase and rutile as a minor phase. As the amount of HNO_3 in the precursor solution increased, the formation of anatase phase was promoted as indicated by an increase of the anatase peak upon increasing acid content. In the case of Sol_2A the ratio of anatse to rutile was 65:35. The phase ratio changed to 70:30 and 95:05 when the amount of acid used was 3 and 4 ml, respectively. Pure anatase was obtained from Sol_2D in which the solution contained 5 ml of acid (H_2O: EtOH: HNO_3 = 10:10:5). Figure 4.10 shows the relationship between weight fraction of anatase and rutile phases obtained after 20 days of aging and the volume of HNO_3 used in the precursors (i.e., 2, 3, 4 and 5 ml). This figure clearly reveals that the increase in concentration of HNO_3 resulting in the product having higher amount of anatase phase. Note that an amorphous phase was expected to be present in all samples as the XRD patterns had high background.

As described in the above result, the effect of the concentration of HNO_3 added for accelerating the hydrolysis reaction was clearly investigated. The phases appeared in the TiO_2 powders were influenced by the amount of HNO_3 added in the TiO_2 sol precursor. It was shown that the high content of HNO_3 added in the TiO_2 sol precursor resulted in the anatase structure. The coexistence of anatase and rutile phases was formed between 2 and 4 ml of HNO_3. Previous reports suggested that TiO_2 normally existed as a sixfold coordinated $[Ti(H_2O)_6]^{4+}$ complex. It was known that the formation of both anatase and rutile can grow from TiO_6 octahedra, and the phase transformation was performed by the rearrangement of the octahedra. In the case of anatase, TiO_2 octahedra preferred to form edge-sharing structure [5]. As mentioned previously, the degree of hydrolysis reaction was

promoted by the addition of H_2O, HCl and HNO_3 (hydrolysis catalysts). Therefore, it led to the dramatically decreasing of the amount of residual alkyls by the replacement of OH^- groups. The more replacement of alkyl groups by OH^-, the greater appearance of anatase phase was. The concentration of OH^- preventing the reconstruction of Ti-O octahedron was huge, resulting in the forming of anatase phase.

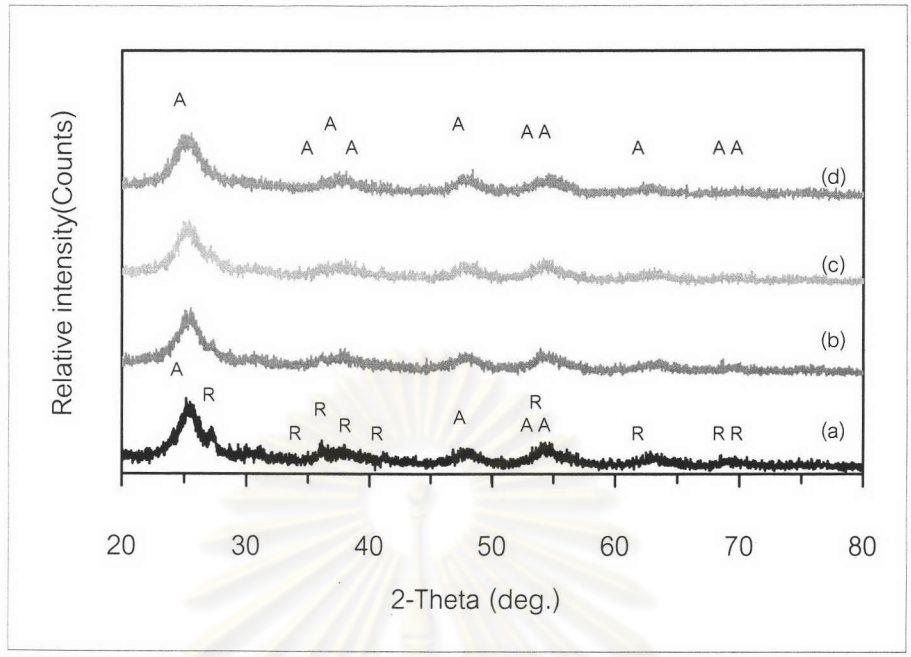

Figure 4.9 XRD patterns of the as-synthesized powders obtained from TiO_2 precursors with the different ratio of H_2O: EtOH: HNO_3, 20 days of aging time; (a) Sol_2A (10:10:2), (b) Sol_2B (10:10:3), Sol_2C (10:10:4) and Sol_2D (10:10:5); A = Anatase, R = Rutile

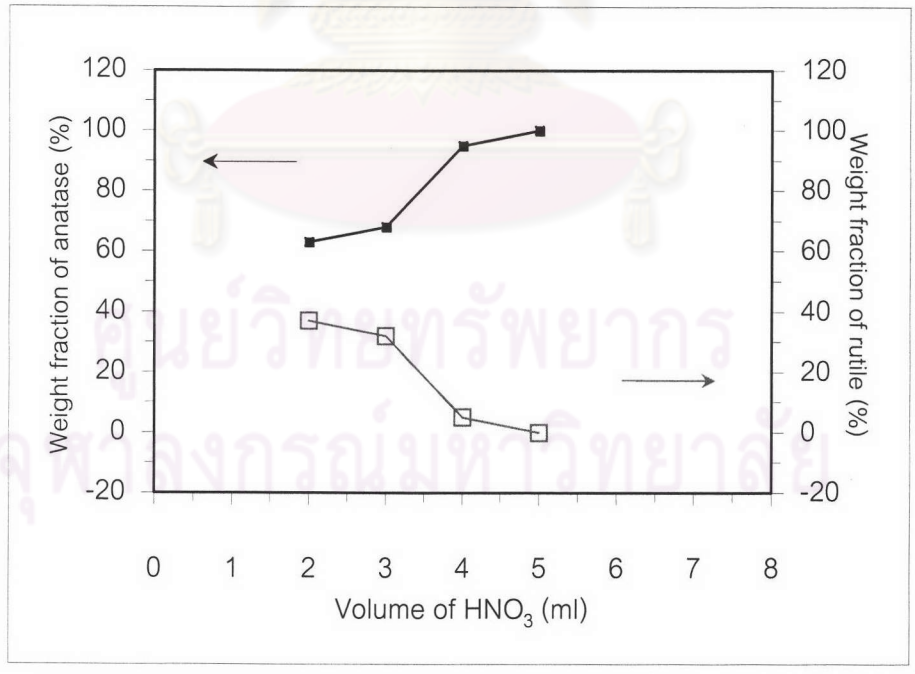

Figure 4.10 The weight fraction of anatase and rutile as a function of volume of HNO_3 (2, 3, 4 and 5 ml) obtained from TiO_2 precursors with the 20 days of aging time

In order to further investigate the effect of aging time on phase formation of the TiO_2 with the present of HNO_3 catalyst, Sol_2A (H_2O: EtOH: HNO_3 = 10:10:2) was aged for different times. This sample was selected according to the preliminary experiment which showed that both anatase and rutile phases appeared at medium aging time. Figure 4.11 shows X-ray diffraction patterns of the as-synthesized powders obtained from Sol_2A aged for 10 – 50 days. At the early stage of aging time (10 days, Figure 4.11(a)), the powder consisted of anatase together with the tiny peak of rutile phase. Upon increasing of aging time, the intensity of the peak corresponding to the anatase phase decreased, while that of the rutile phase increased as shows in Figure 4.11(a) – (e). The change of peak intensity observed in the powder obtained from the Sol_2A was in lesser extent than those observed in the powder obtained from the Sol_1A and Sol_1E in which the HCl catalyst was used (Figure 4.2 and 4.3).

The above results clearly showed that the aging time had pronounced effect on the phase present in the TiO_2 sol. The transformation of anatase and rutile phase had also been observed from the sol aged for a long time at room temperature [5]. It was believed that the Ti-O octahedra of the anatase phase reconstructed to the rutile phase. For prolonged aging time, the residual alkyl groups were marginally declined when the hydrolysis catalysts (HNO_3 and H_2O) was added into the TiO_2 sol precursor. The disappearance of residual alkyl groups promoted the transformation of Ti-O octahedra.

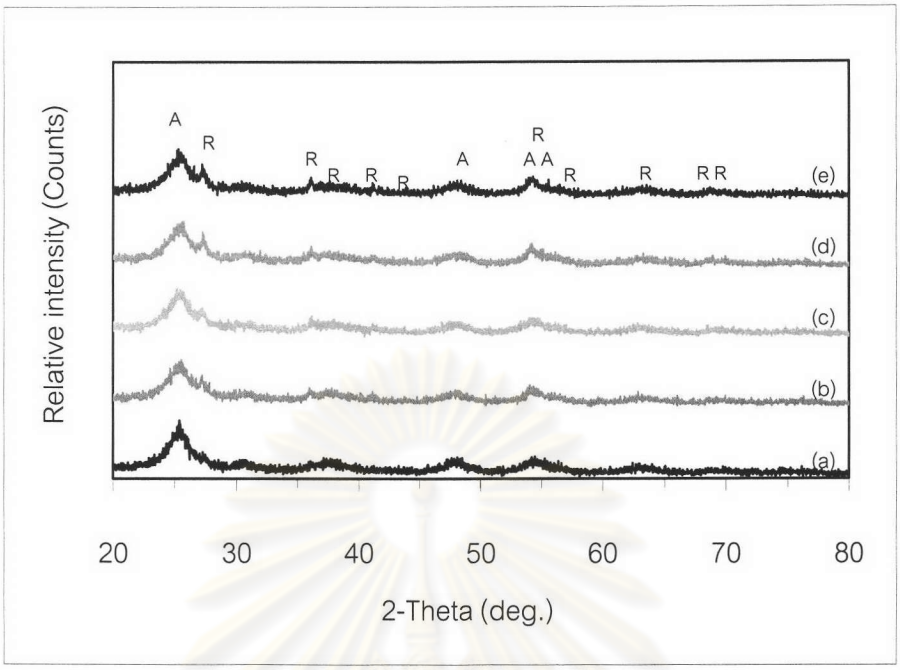

Figure 4.11 XRD patterns of the as-synthesized powders obtained Sol_2A (H_2O: EtOH: HNO_3 = 10:10:2) aged for (a) 10 days, (b) 20 days, (c) 30 days, (d) 40 days and (e) 50 days

To compare the effect of HCl and HNO_3 catalysts on the phase formation, XRD pattern acquired from Sol_2E (HCl catalyst) and from Sol_2A (HNO_3 catalyst) both aged for 50 days were plotted in comparison, and the result is shown in Figure 4.12. For the XRD pattern acquired from the TiO_2 powder obtained from Sol_2E (H_2O: EtOH: HCl = 10:10:2.6, Figure 4.12(a)), the rutile phase was predominated (anatase: rutile = 30:70). In the case of the pattern acquired from the TiO_2 powder obtained from Sol_2A (H_2O: EtOH: HNO_3 = 10:10:2, Figure 4.12(b)), the phase composition was 55% anatase and 45% rutile.

By comparing of these two samples that used different kinds of hydrolysis catalyst, it was evident that HCl catalyst promoted the formation of rutile phase while HNO_3 catalyst promoted the formation of the anatase phase. The role of each catalyst can be described as follow. It has been realized that the addition of HCl, HNO_3 and H_2O accelerated the hydrolysis rate of the alkoxide precursor. A quantity of this hydrolysis catalyst must be sufficient to hydrolyze the $Ti(OC_4H_9)$ completely [5]. Generally, the greater degree of

hydrolysis is the result of the complete hydrolysis of the alkyl groups. When adding HCl as a hydrolysis catalyst, the amount of residual alkyls that would prevent the reconstruction of Ti-O octahedra to rutile is small, so the resulted microstructure resembles that of the rutile phase. The rutile structure is the most stable phase in the low-pH solution [20]. In the same manner, adding the HNO_3 as a hydrolysis catalyst result to the slow hydrolysis rate. Consequently, the concentration of residual alkyls preventing the reconstruction of Ti-O octahedra to rutile is huge, resulting in the forming of anatase phase.

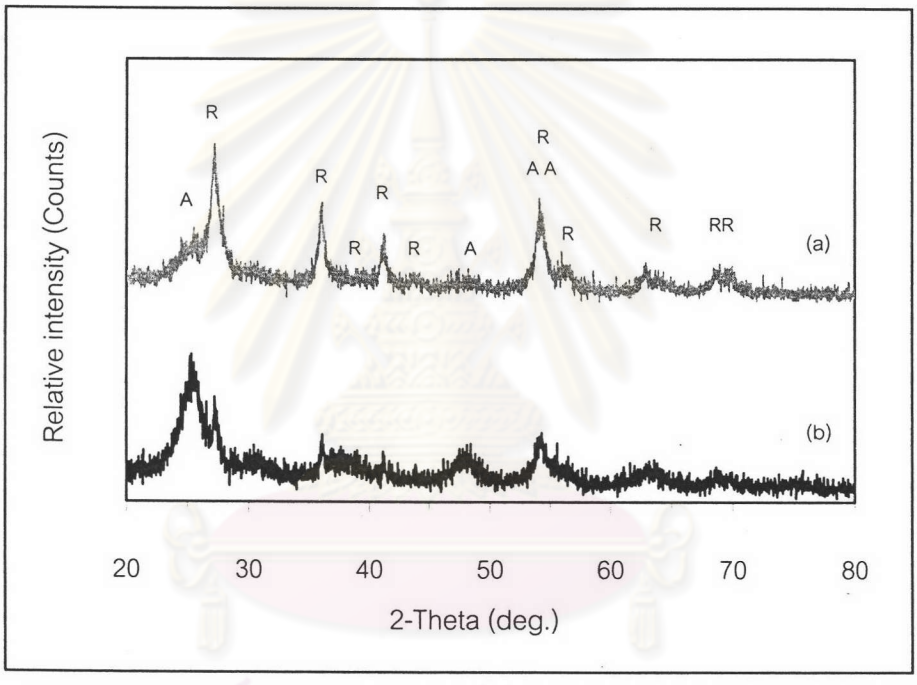

Figure 4.12 XRD patterns of the as-synthesized powders obtained from; (a) Sol_2E (HCl catalyst), and (b) Sol_2A (HNO_3 catalyst) aged for 50 days; A = Anatase, R = Rutile

To study thermal stability of the prepared TiO_2, the samples obtained from Sol_2D (H_2O: EtOH: HNO_3 = 10:10:5, 20 days aging) were calcined in air at various temperatures (300, 400, 500, 600 and 700°C) for 4 h. Figure 4.13 shows the XRD pattern of the as-synthesized TiO_2 powders compared with those of the calcined powders at different temperatures. According to these results, the as-synthesized powder from the solution condition specified contained only anatase phase along with amorphous phase (Figure 4.13(a)). After calcined at 300 and 400°C (Figure 4.13(b,c)), phase composition observed at these temperatures were also only anatase, and the powders contained a well defined crystalline TiO_2 nanoparticles as indicated by sharper peaks. Moreover, it was found that the rutile phase firstly appeared at 500°C (Figure 4.13(d)). The phase ratio of the anatase-rutile was slightly decreased when calcined at 600°C (Figure 4.13(e)) and completely transformed to rutile phase at 700°C (Figure 4.13(f)). The plot of weight fraction of anatase and rutile derived from XRD pattern using Eq. (3.1) and (3.2) as a function of calcination temperatures obtained from Sol_2D with the 20 days of aging time is shown in Figure 4.14. It was clearly seen that anatase-to-rutile phase transformation took place at temperature above 400°C. The crystallite sizes of TiO_2 photocatalysts were estimated using Eq. (3.3) and summarized in Table 4.3. It was obvious that increasing calcination temperature caused the crystallite growth and anatase-to-rutile phase transformation. The crystallite growth resulted in the decrease of specific surface area. Many researchers have reported that the transformation of metastable anatase phase to the most stable rutile phase occurred at a temperature above 700°C [27]. The phase transformation temperature observed from the TiO_2 synthesized in this work was much lower, probably due to very fine crystallite size.

Thermal stability of the TiO_2 prepared from Sol_2C (H_2O: EtOH: HNO_3 = 10:10:4, 20 days aging) was also studied, and the XRD result is shown in Figure 4.15. Thermal behavior of this sample was similar to the sample obtained from the Sol_2D. That was, heat treatment promoted the transformation of anatase to rutile phase, and resulted in the increase of crystallinity. The phase ratios, as well as the crystallite size, of the samples described above are listed in Table 4.3.

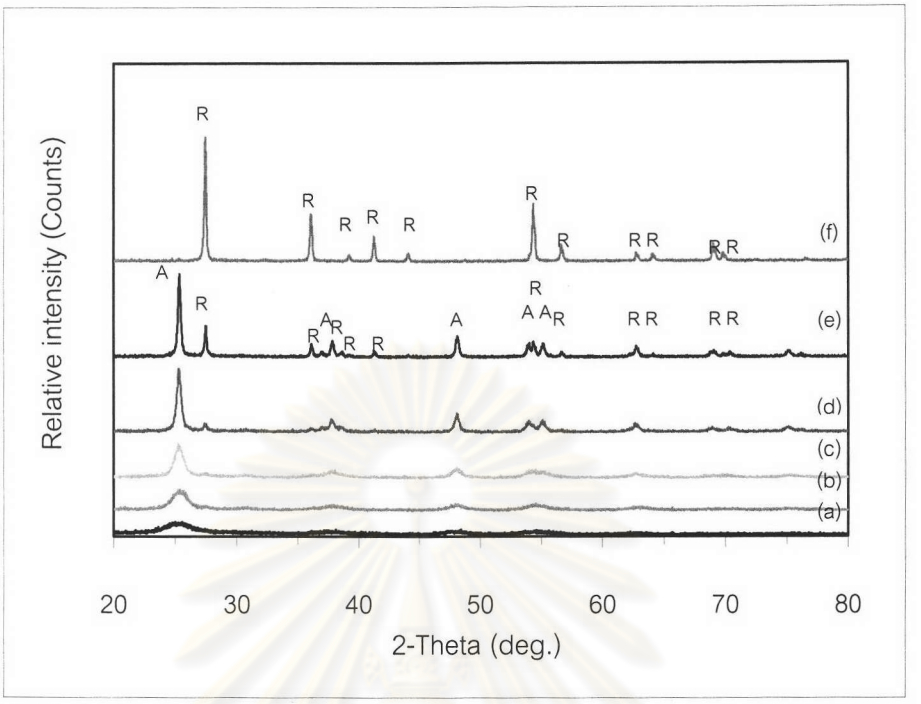

Figure 4.13 XRD patterns of the as-synthesized powders obtained from Sol_2D (H_2O: EtOH: HNO_3 = 10:10:5) with the 20 days of aging time and calcined at; (a) as-synthesized, (b) 300 °C, (c) 400 °C, (d) 500 °C, (e) 600 °C and (f) 700°C, 4 h in air; A = anatase, R = rutile

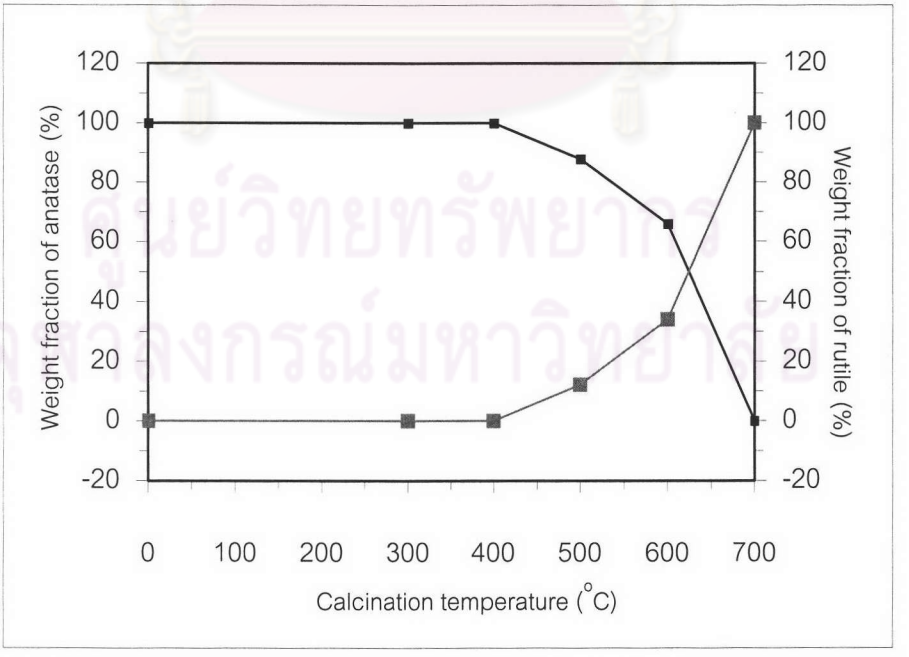

Figure 4.14 The weight fraction of anatase and rutile as a function of calcination temperatures obtained from Sol_2D with the 20 days of aging time

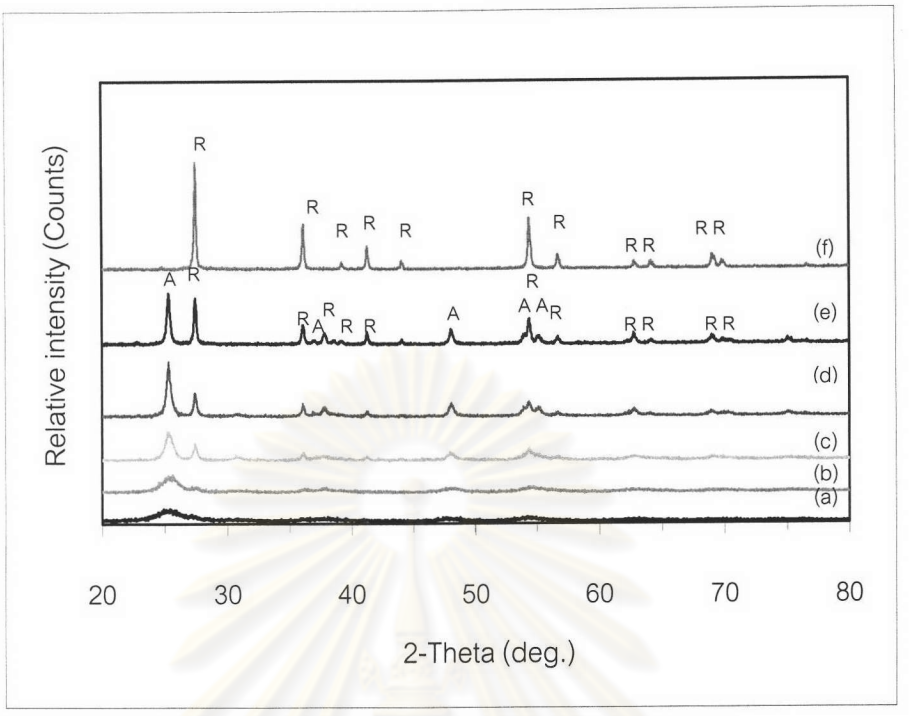

Figure 4.15 XRD patterns of the as-synthesized powders obtained from Sol_2C (H_2O: EtOH: HNO_3 = 10:10:4) with the 20 days of aging time and calcined at; (a) as-synthesized, (b) 300 °C, (c) 400 °C, (d) 500 °C, (e) 600 °C and (f) 700°C, 4 h in air; A = anatase, R = rutile

To investigate the effect of calcination time on rate of phase transformation, the TiO_2 powders obtained from Sol_2D (H_2O: EtOH: HNO_3 = 10:10:5) were calcined at 500°C for 4, 7, and 10 h. XRD patterns are shown in Figure 4.16. It was obvious that the phase ratio of anatase to rutile was gradually decreased with increasing calcination time. The phase ratio decreased from 90:10 (4 h) to 75:25 (7 h) and to 70:30 (10 h), respectively. However, it was evident that the calcination time had no pronounced effect on the phase transformation. The phase composition and crystal size of the samples calcined at various calcination times are listed in Table 4.3.

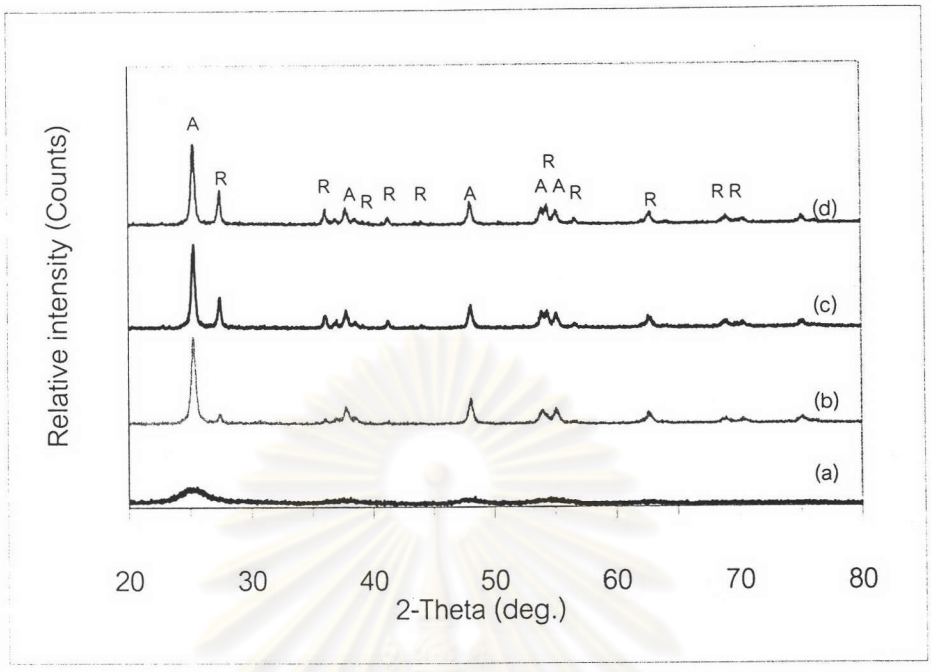

Figure 4.16 XRD patterns of the as-synthesized powders obtained from Sol_2D (H_2O: EtOH: HNO_3 = 10:10:5) calcined at 500°C with different calcination time; (a) as-synthesized, (b) 4 h, (c) 7 h and (d) 10 h

The specific surface areas of the as-synthesized TiO_2 powders obtained from different precursors were found to be different. For instance, by comparison the sample obtained from the Sol_2C and Sol_2D, the specific surface area of the powder obtained from Sol_2D was larger than that of the powder obtained from Sol_2C. The BET surface areas are listed in Table 4.3. The difference of the specific surface area of the two samples could be a result of the different amounts of HNO_3 present in the precursor solution [21]. The TiO_2 powders prepared under high HNO_3 concentration, protons (H^+) from the HNO_3 were adsorbed on the surface of the primary particles. So most particles carried positive charge and repelled each other to form a stable sol. On the other hand, the powders prepared under low HNO_3 concentration, highly aggregated clusters of the primary particles occurred. Since the powders prepared with excess HNO_3 had fewer aggregates and the powders were packed more uniformly, the specific surface area was higher. The above results were again confirmed by SEM observation as shown in Figure 4.17. It was also apparent that the specific surface area shifted towards smaller values at higher calcination temperatures since the particles aggregated. The uncalcined sample obtained from Sol_2D

possessed high specific surface area (239.3 m^2/g), which then decreased to 5.7 m^2/g when calcined at 700°C.

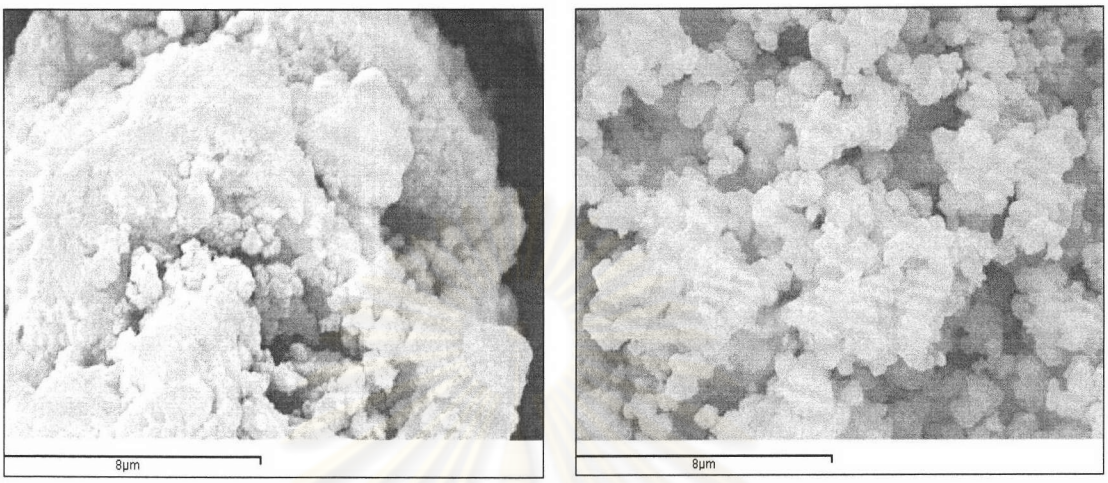

(a) (b)

Figure 4.17 SEM images of as-synthesized TiO_2 powders obtained from TiO_2 precursors with the different ratios of H_2O: EtOH: HNO_3, 20 days of aging time; (a) Sol_2C, (b) Sol_2D

Figures 4.18-4.23 are TEM micrographs of the TiO_2 powders obtained from Sol_2C calcined at various temperatures showing anatase and rutile crystals of different average size as a function of calcination temperature. It was clearly observed that increasing calcination temperature caused the crystal growth and also resulted in a well-defined crystal. The average crystallite sizes at various calcination temperatures are summarized in Table 4.3.

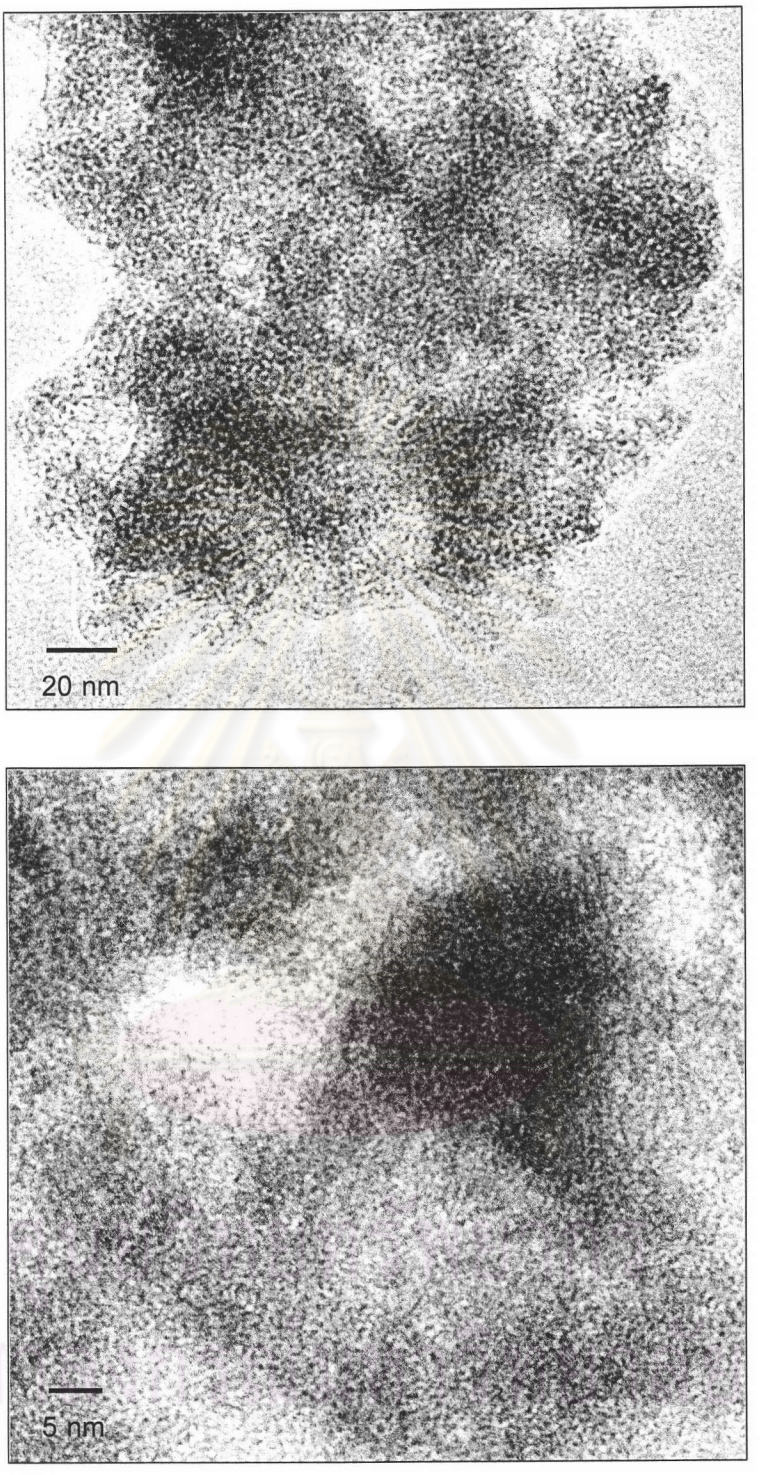

Figure 4.18 TEM images of as-synthesized TiO_2 powders obtained from Sol_2C (H_2O: EtOH: HNO_3 = 10:10:4) aged for 20 days

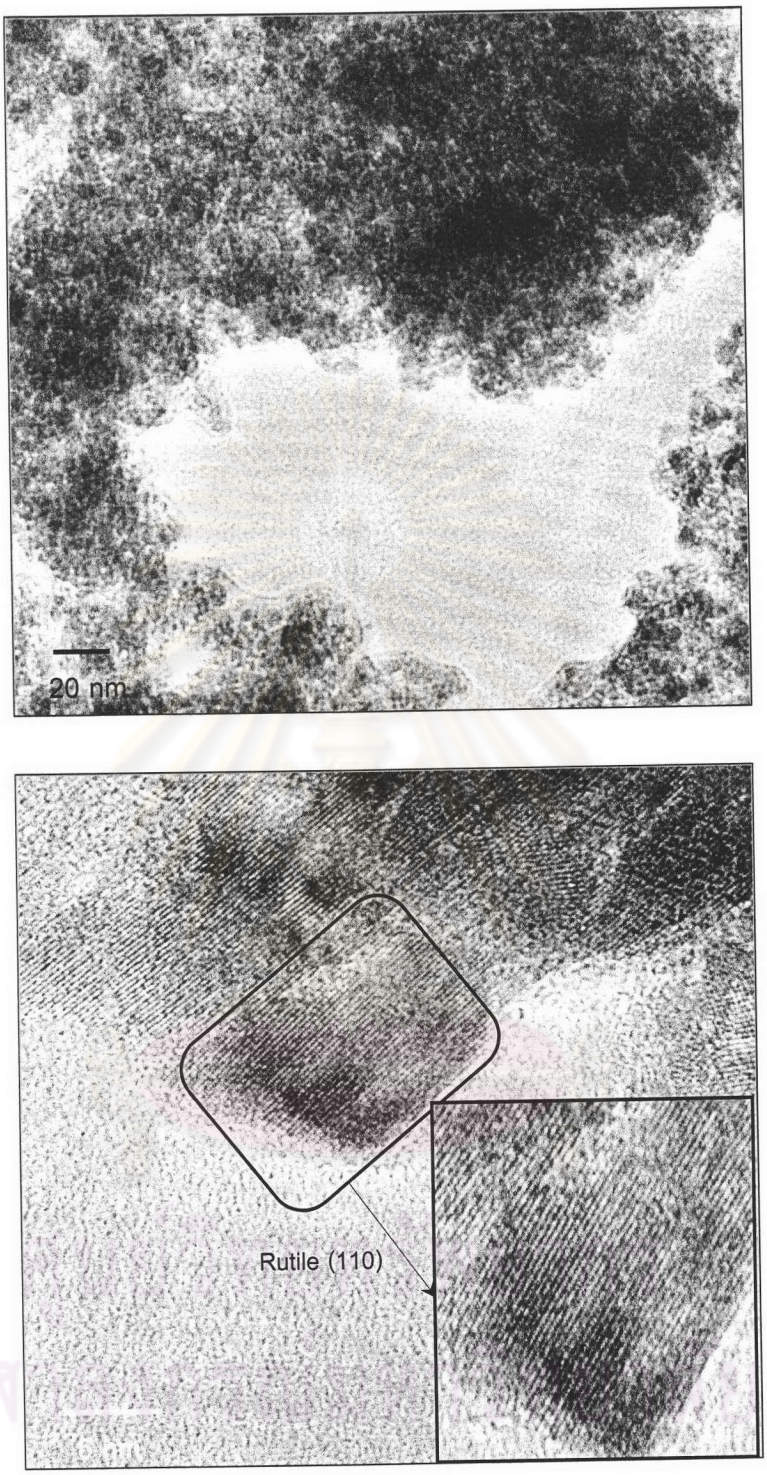

Figure 4.19 TEM images of TiO_2 powders obtained from Sol_2C (H_2O:EtOH:HNO_3 = 10:10:4) aged for 20 days and calcined at 300°C for 4h (Inset shows d-spacing of 3.0 Å corresponding to (110) plane of rutile)

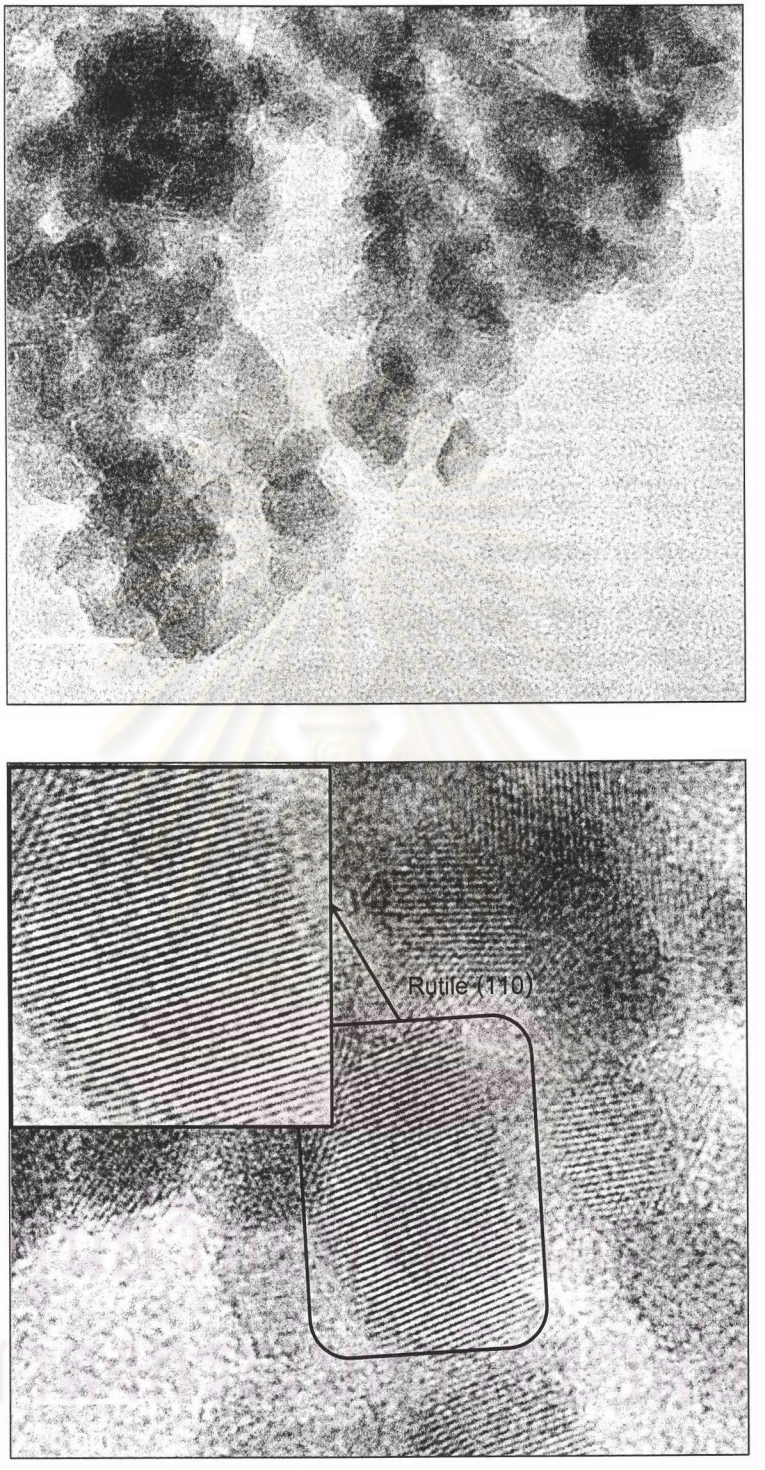

Figure 4.20 TEM images of TiO_2 powders obtained from Sol_2C (H_2O:EtOH:HNO_3 = 10:10:4) aged for 20 days and calcined at 400°C for 4h (Inset shows d-spacing of 3.2 Å corresponding to (110) plane of rutile)

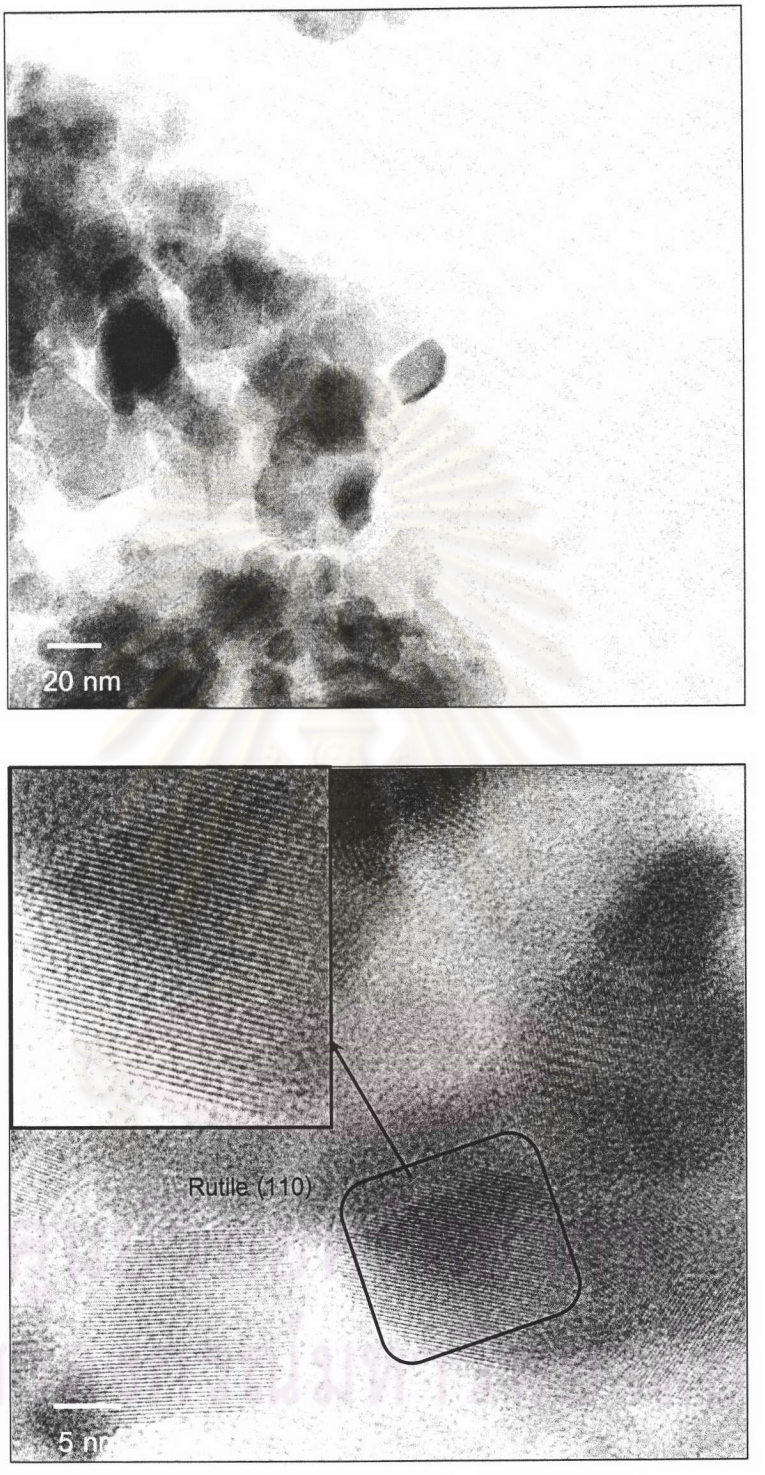

Figure 4.21 TEM images of TiO_2 powders obtained from Sol_2C (H_2O:EtOH:HNO_3 = 10:10:4) aged for 20 days and calcined at 500°C for 4h (Inset shows d-spacing of 3.3 Å corresponding to (110) plane of rutile)

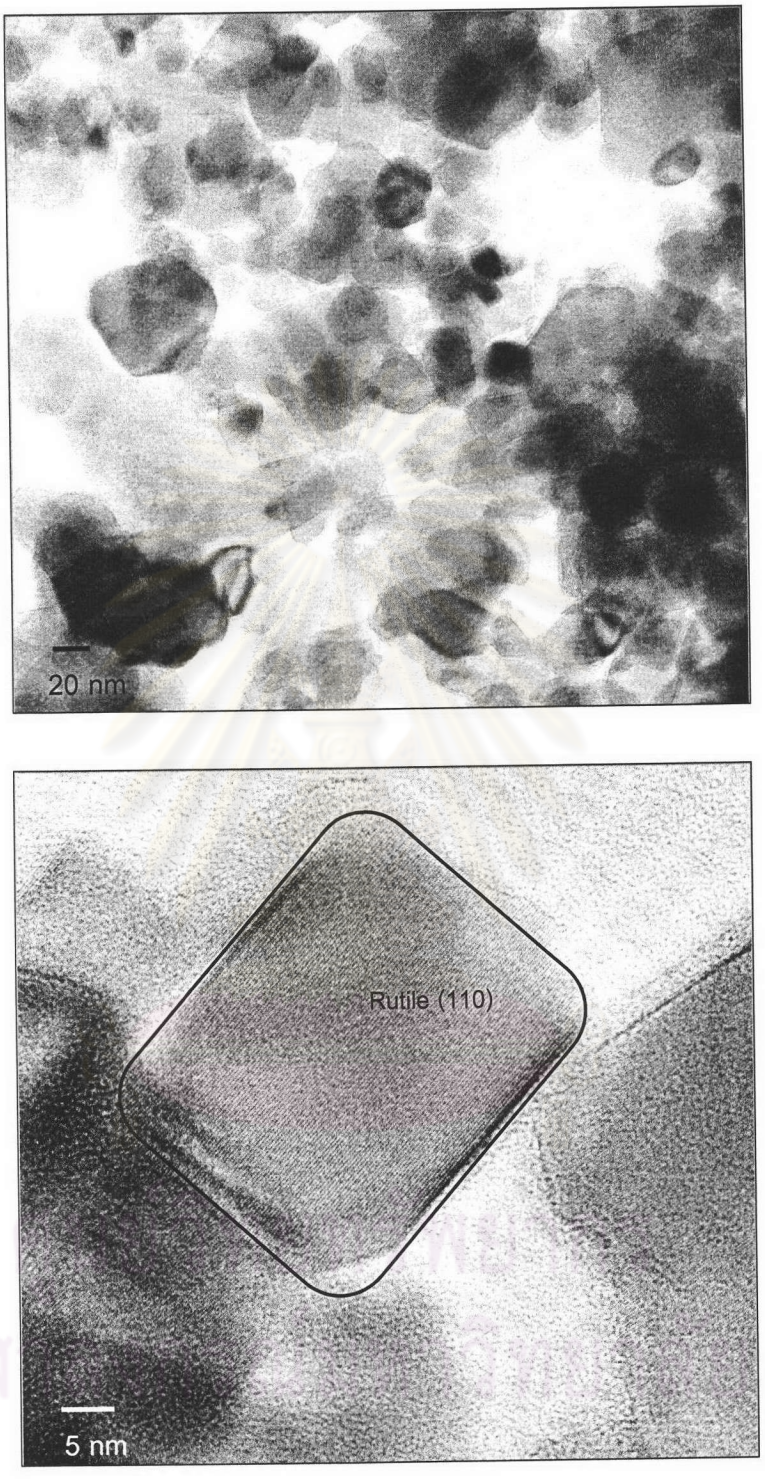

Figure 4.22 TEM images of TiO_2 powders obtained from Sol_2C (H_2O:EtOH:HNO_3 = 10:10:4) aged for 20 days and calcined at 600°C for 4h (Inset shows d-spacing of 3.3 Å corresponding to plane (110) of rutile)

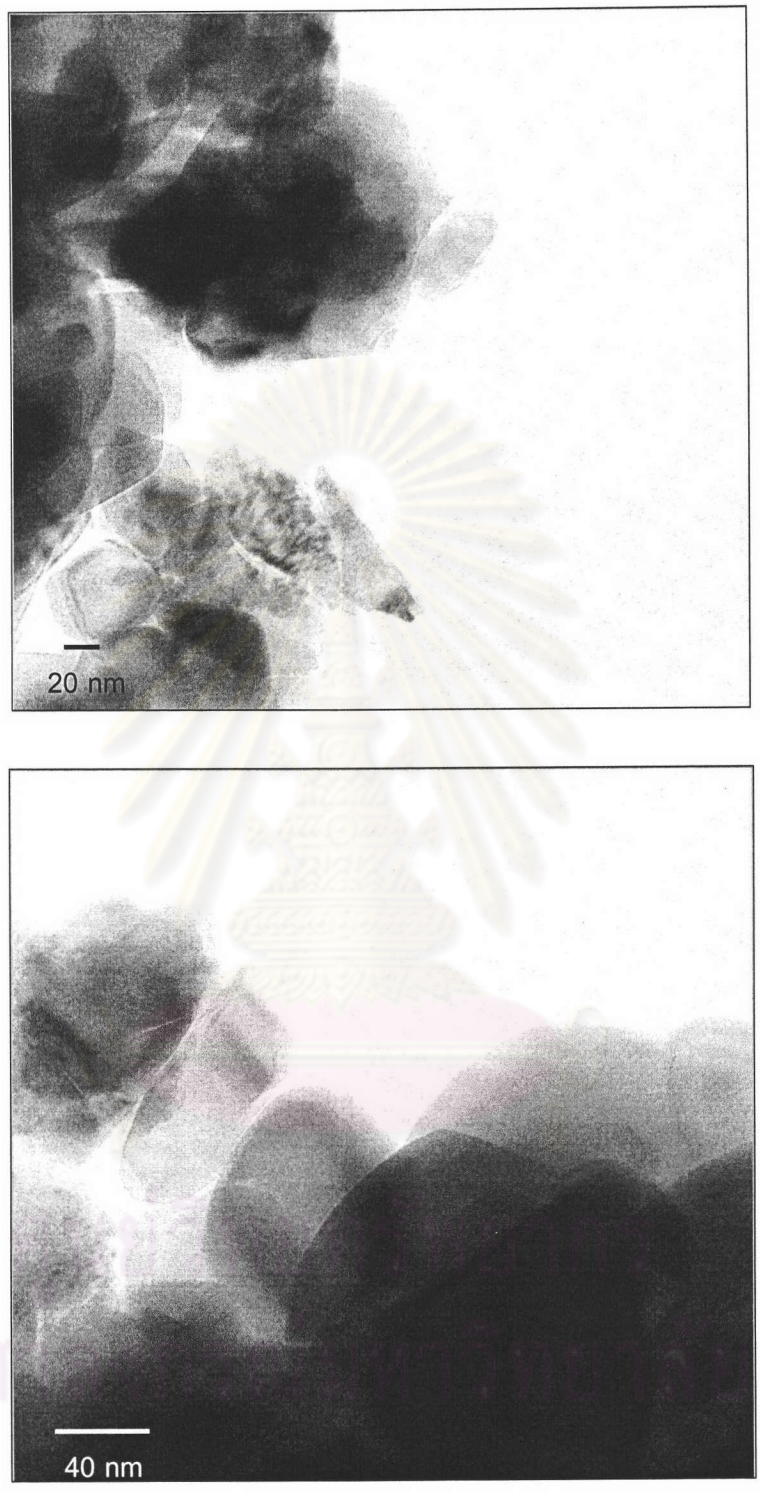

Figure 4.23 TEM images of TiO_2 powders obtained from Sol_2C (H_2O:EtOH:HNO_3 = 10:10:4) aged for 20 days and calcined at 700°C for 4h

Table 4.3 Phase composition, crystallite size and specific surface area of the TiO_2 powders obtained from Sol_2C and Sol_2D calcined at various temperatures compared to those of commercial powder, Degussa P-25

Samples	Calcination temperature (°C)	Phase composition (A: R)	Crystallite size[a] (nm.)		Crystallite size[b] (nm.)		Surface area (m^2/g)
			d_A	d_R	d_A	d_R	
Sol_2C	Noncalcined	100:0	4	-	3	-	168
Sol_2C_300_4h	300	75:25	6	20	4x7	11x15	152
Sol_2C_400_4h	400	70:30	12	33	6x10	10x17	61
Sol_2C_500_4h	500	60:40	21	36	14x19	23x20	38
Sol_2C_600_4h	600	46:54	31	49	-	31x43	25
Sol_2C_700_4h	700	0:100	-	60	-	54x118	7
Sol_2D	Noncalcined	100:0	3	-	-	-	239
Sol_2D_300_4h	300	100:0	7	-	-	-	116
Sol_2D_400_4h	400	100:0	11	-	-	-	75
Sol_2D_500_4h	500	90:10	23	40	-	-	26
Sol_2D_500_7h	500	75:25	27	34	-	-	-
Sol_2D_500_10h	500	70:30	28	34	-	-	-
Sol_2D_600_4h	600	65:35	35	53	-	-	7
Sol_2D_700_4h	700	0:100	-	58	-	-	6
P-25	-	85:15	23	31	-	-	50

a = calculated from XRD peaks

b = directly measured from TEM images

4.1.2 V-doped TiO_2

Figure 4.24 shows the XRD patterns of the as-synthesized V-doped TiO_2 obtained from Sol_2D (H_2O: EtOH: HNO_3 = 10:10:5) containing various amount of V dopant (0.01, 0.05, 0.1 and 0.2 % V) aged for 20 days and dried at 45°C for 1 day. In all samples, only anatase phase was observed. Calcination at 300°C for 4 h barely caused phase transformation. At the calcination temperature of 400°C (4 h), anatase-to-rutile phase transformation was observed, particularly in the sample containing low V content as shown in Figure 4.25. At higher V content, the rutile peaks were barely seen. This result indicates that the V dopant inhibited the anatase-to-rutile phase transformation. Note that the corresponding peaks of V or vanadium oxides such as V_2O_5 or VO_2 were not present in the XRD patterns since the content was below detection limit, or they could present in amorphous state. The crystallite size and phase composition of the V-doped TiO_2 were also derived from the XRD pattern. These results were again confirmed by TEM analysis as shown in Figure 4.26. It is indicated that by adding V dopant the crystallize size of TiO_2 photocatalyst was not different. The vanadium or vanadium oxide grains were not clearly observed in TEM analysis. The results are summarized in Table 4.4.

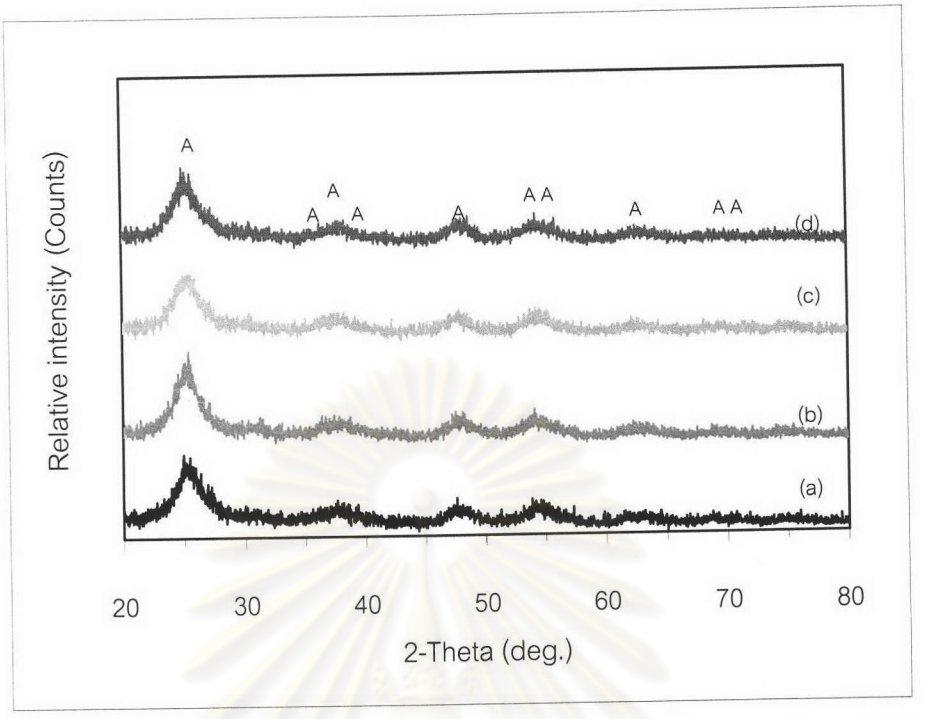

Figure 4.24 XRD patterns of the as-synthesized, V-doped TiO_2 powders obtained from Sol_2D (H_2O: EtOH: HNO_3 = 10:10:5) containing various amount of V dopant aging at 20 days (a) 0.01%V, (b) 0.05%V, (c) 0.10%V and (d) 0.20%V; A = anatase, R = rutile

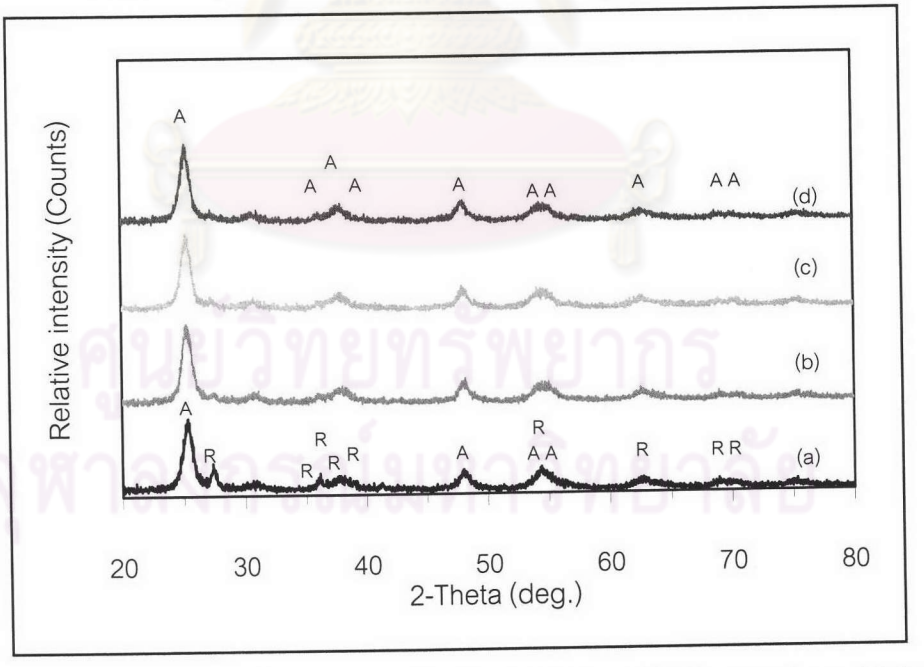

Figure 4.25 XRD patterns of the as-synthesized, V-doped TiO_2 powders obtained from Sol_2D (H_2O: EtOH: HNO_3 = 10:10:5) containing various amount of V dopant aged for 20 days and calcined at 400°C, 4 h; (a) 0.01%V, (b) 0.05%V, (c) 0.10%V and (d) 0.20%V; A = anatase, R = rutile

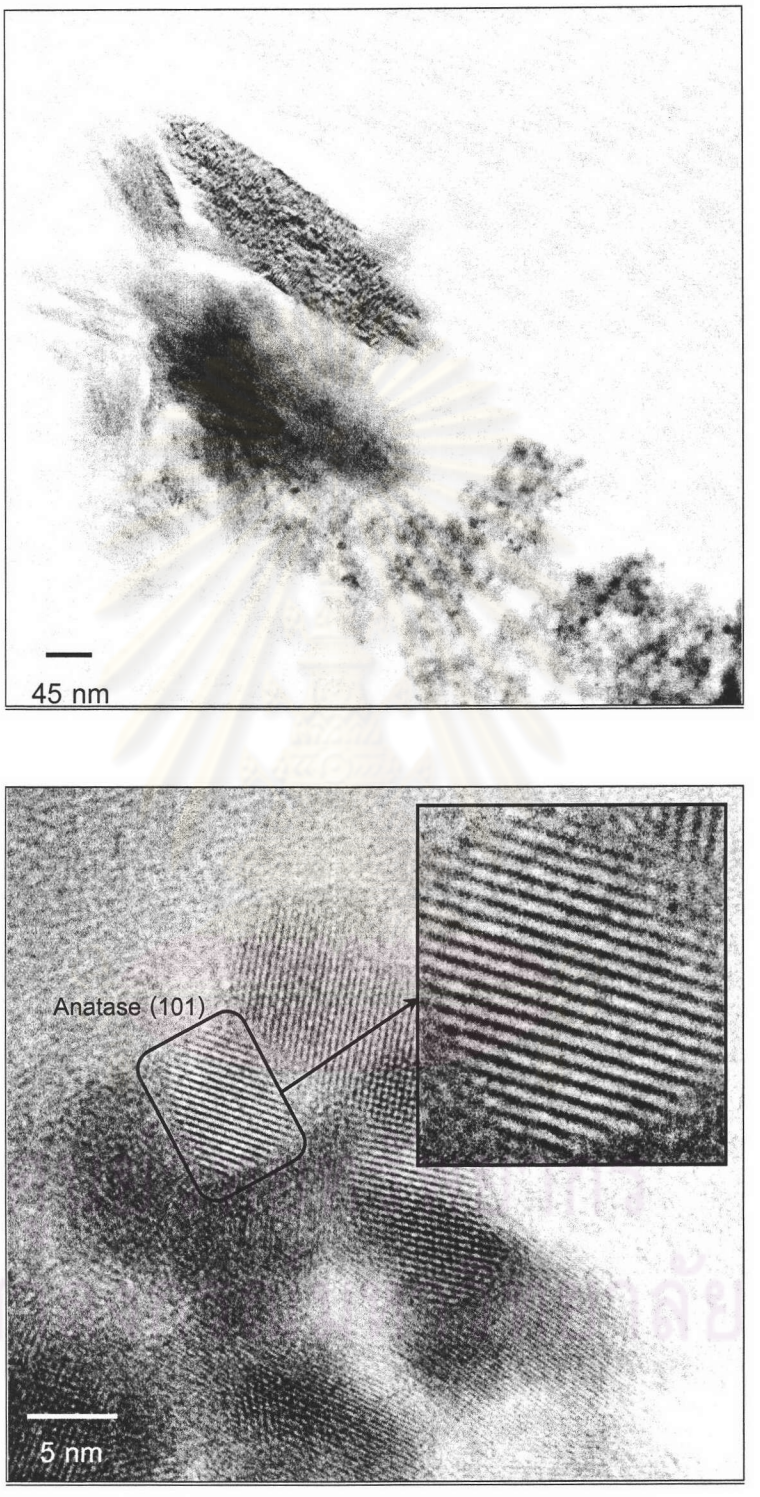

Figure 4.26 TEM images of V-doped TiO_2 powders obtained from Sol_2D (H_2O:EtOH:HNO_3 = 10:10:5) with 0.20%V calcined at 400°C for 4h (Inset shows d-spacing of 3.41 Å corresponding to plane (101) of anatase)

Table 4.4 Phase composition and crystallite size of the V-doped TiO_2 powders obtained from Sol_2D at different concentrations of V dopant calcined at 400°C, 4 h

Samples code	Phase composition (A: R)	Crystallite size[a] (nm)		Crystallite size[b] (nm)	
		d_A	d_R	d_A	d_R
Sol_2D_0.01V	85:15	4	10	-	-
Sol_2D_0.05V	95:05	6	10	-	-
Sol_2D_0.10V	96:04	8	10	-	-
Sol_2D_0.20V	97:03	8	11	9x11	9x13

a = calculated from XRD peaks

b = directly measured from TEM images

Since the presence of vanadium dopant was not directly observed by XRD analysis, an elemental analysis using an energy dispersive X-ray spectroscope (EDS) equipped to the SEM unit was performed. For EDS analysis, the TiO_2 sample having relatively high V content was specially prepared to ensure that the V content exceeded detection limit of the EDS detector. High V loading also resulted in more accurate mapping result since the V mapping was performed by using the $K\beta$ line of the V (which has low intensity) at 5.4 KeV instead of using the $K\alpha$ line at 4.9 KeV (which has higher intensity but overlaps with $K\beta$ line of the Ti). Figure 4.27(e) is an EDS spectrum acquired from the 10 wt.% V-doped TiO_2 calcined at 500°C for 4 h. Strong Ti, O, and V peaks were observed. The amount of V dopant measured by EDS was 6.3 %wt, which was smaller than the concentration of V added into the precursor. Figure 4.27(a-d) shows the result of elemental mapping of the Ti, V, O and combined image of all 3 elements. The green color represents the Ti element, while the red one denotes the V dopant. The supplemental blue color indicates the O element. According to the combined image, the V uniformly disperses on the TiO_2 particles. The image also shows agglomerated particles of size ranging from 5 to 20 μm.

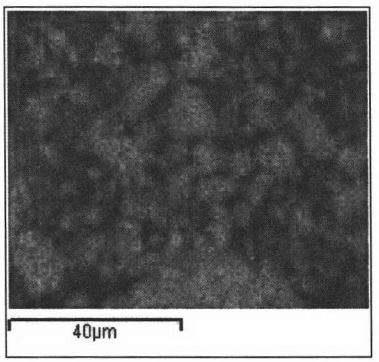

(a: Ti element)

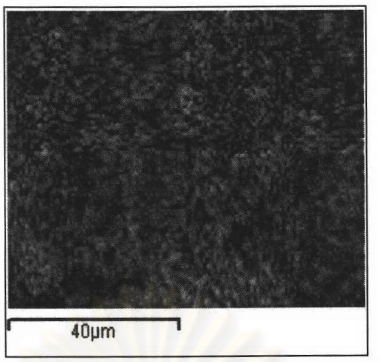

(b: V element)

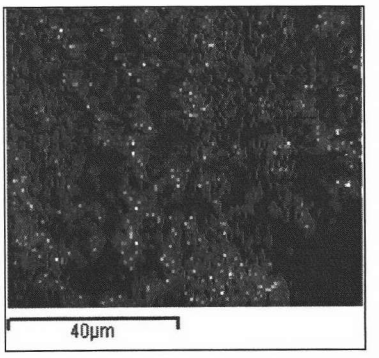

(c: O element)

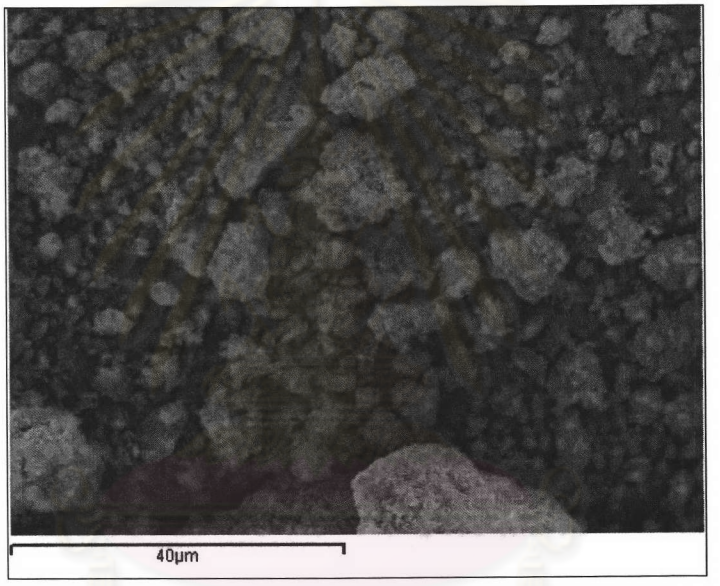

(d: overall image)

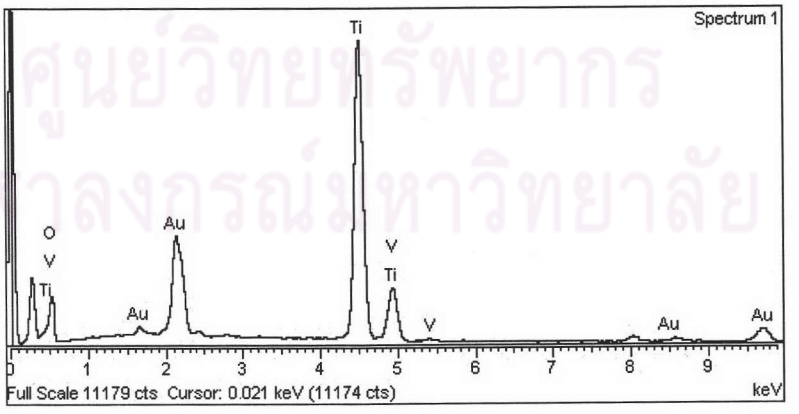

(e: EDS spectrum)

Figure 4.27 Elemental mapping of V-doped TiO_2 powders obtained from Sol_2D as 10.0% V dopant calcined at 500°C, 4 h; (a) Ti element, (b) V element, (c) O element (d) overall image, and (e) EDS spectrum

Elemental mapping was also performed on the sample containing low content of V dopant (0.2 %wt. V) as shown in Figure 4.28. This sample was obtained from Sol_2D, and calcined at 400°C for 4 h.

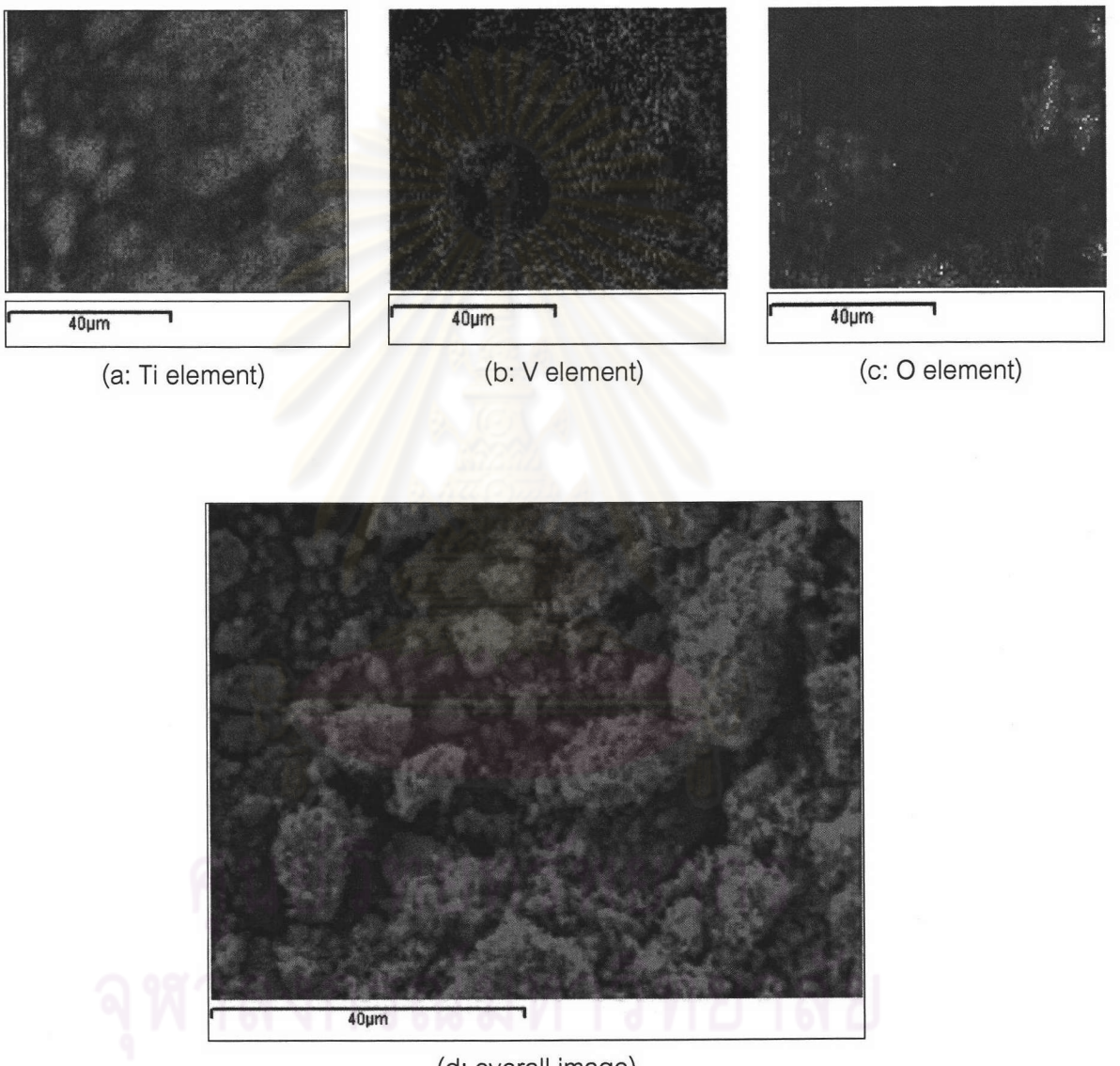

(a: Ti element) (b: V element) (c: O element)

(d: overall image)

Figure 4.28 Elemental mapping of V-doped TiO_2 powders obtained from Sol_2D as 0.2% V dopant calcined at 400°C, 4 h; (a) Ti element, (b) V element and (c) O element and (d) overall image

4.2 TiO_2 coating on substrate

4.2.1 TiO_2 coating on Al_2O_3 beads

Figure 4.29 illustrates the SEM images of the cleaned Al_2O_3 beads calcined at 1,700°C. The average size of the spherical Al_2O_3 beads was around 600 μm. The image in Figure (b) clearly shows the porous surface estimated to be around 5-60 μm. The specific surface area of this bead was about 58 m^2/g.

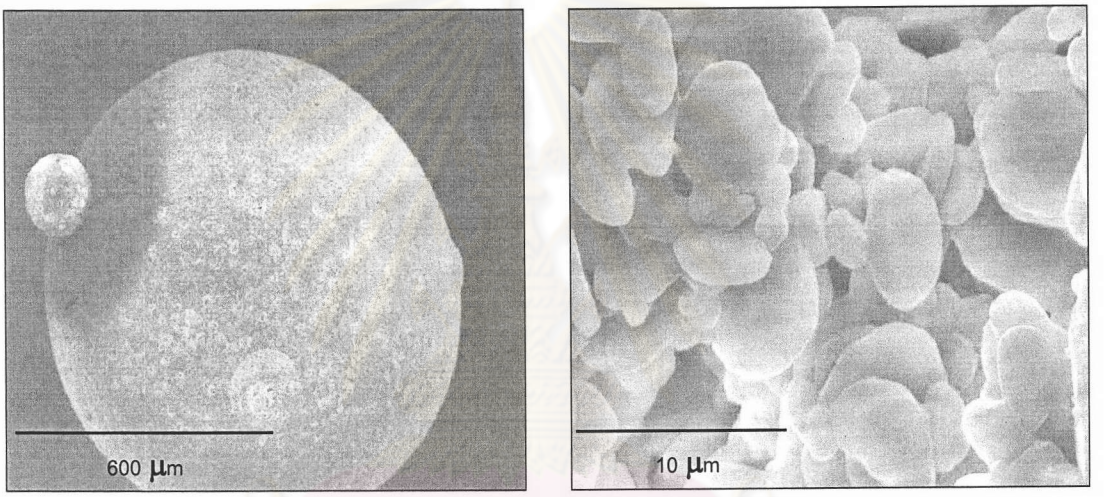

(a) (b)

Figure 4.29 SEM images of Al_2O_3 bead calcined at 1,700°C

Figures 4.30 – 32 show the result of elemental mapping of the TiO_2 coating prepared by soaking the cleaned Al_2O_3 beads into Sol_2C for 1, 3 and 5 times, respectively, and then calcined at 400°C for 4 h. The amount of TiO_2 loading, as well as uniformity, on the bead was found to increase with increasing number of coating cycle. The amount of TiO_2 loading determined by XRF technique was 1.2, 3.5 and 5.3 wt% for 1, 3 and 5 cycle-coating, respectively. The 5 cycle-coated sample was used for photocatalytic study.

Different coating method was carried out by soaking the beads in the sol for 7 days. According to the mapping result (not shown), this coating method gave similar result to the 5-cycle coating in terms of uniform TiO_2 distribution and loading content, which was 5.8 wt%. In this sample, the TiO_2 sol not only dispersed on the outer surface of the Al_2O_3 beads but also penetrated into the pores as shown in Figure 4.33. Table 4.5 shows the amount of TiO_2 loading on the Al_2O_3 beads at the various numbers of coating times (1, 3, 5 and soaking for 7 days).

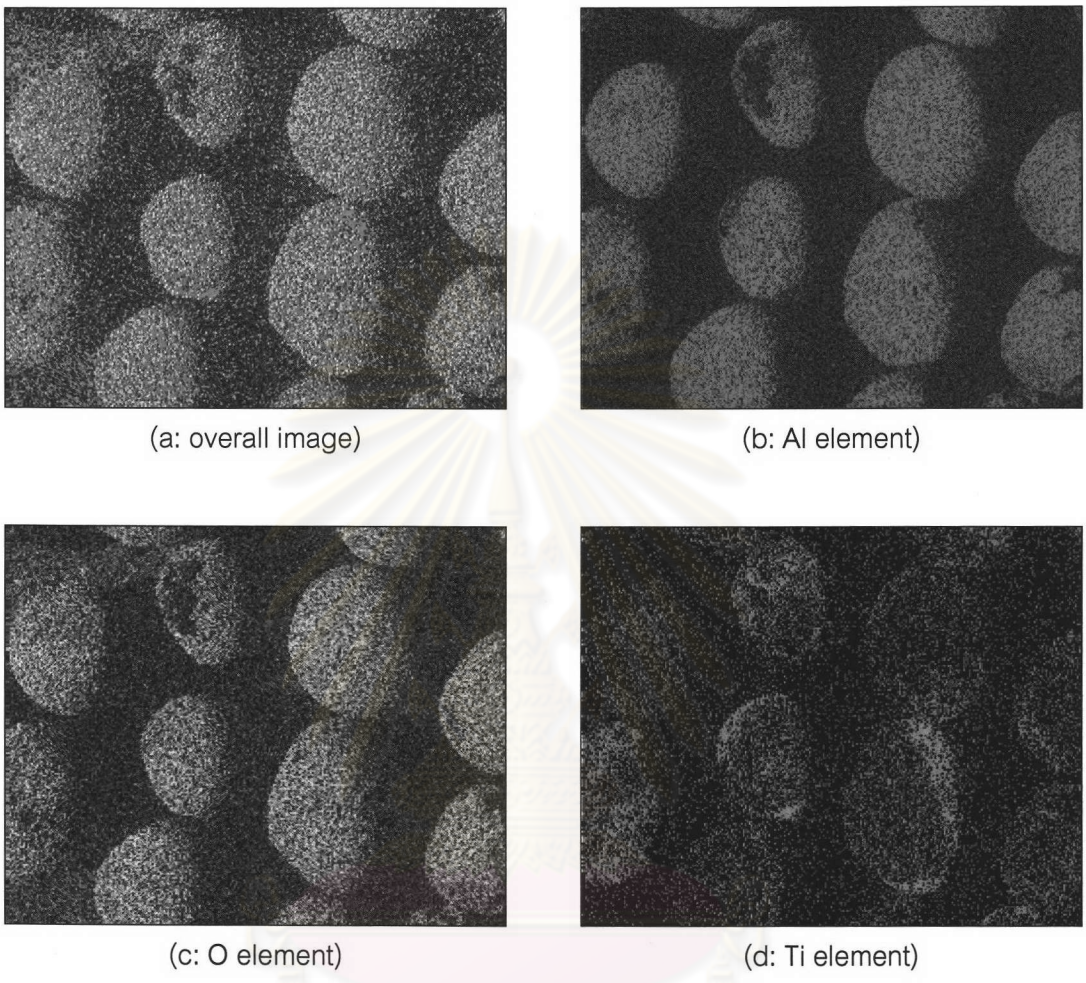

Figure 4.30 SEM images of TiO_2 sol (Sol_2C) coated on Al_2O_3 bead for 1 time and calcined at 400°C for 4 h; (a) overall image, (b) Al element, (c) O element and (d) Ti element

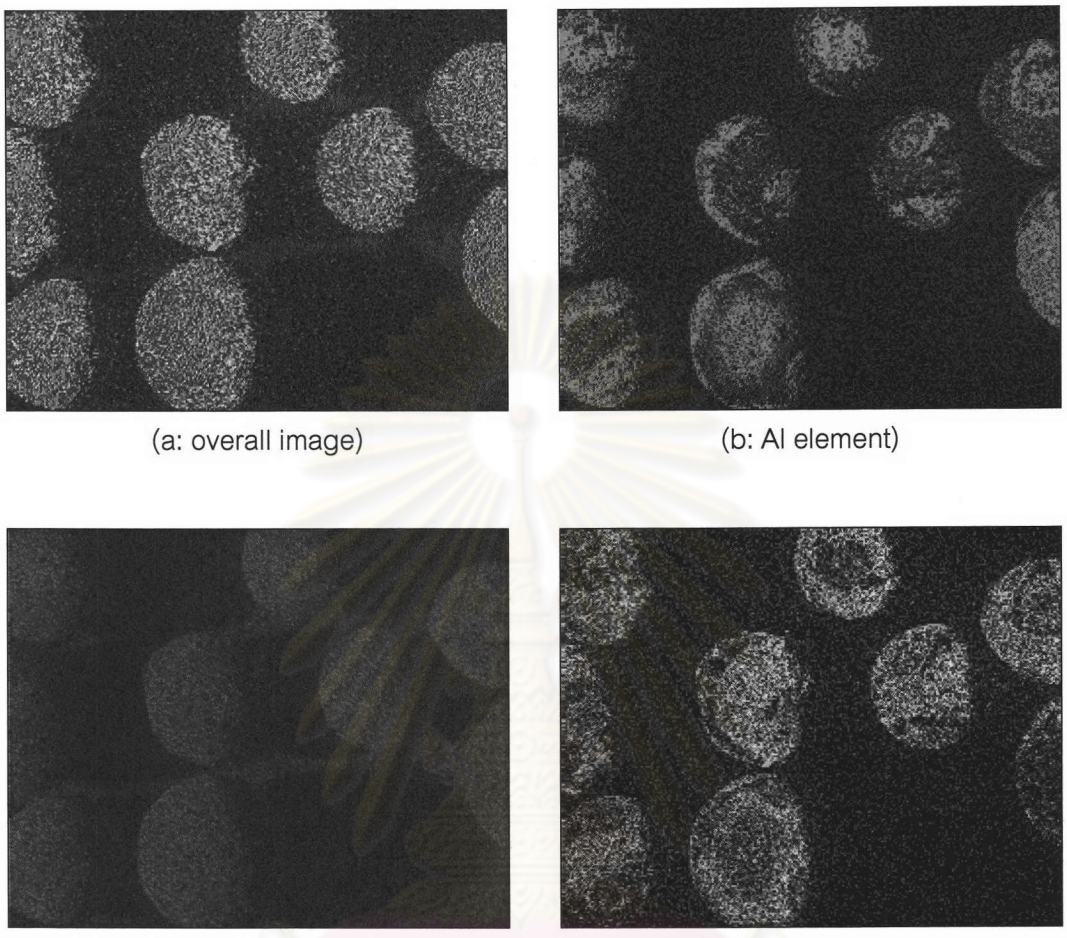

Figure 4.31 SEM images of TiO_2 sol (Sol_2C) coated on Al_2O_3 bead for 3 times and calcined at 400°C for 4 h; (a) overall image, (b) Al element, (c) O element and (d) Ti element

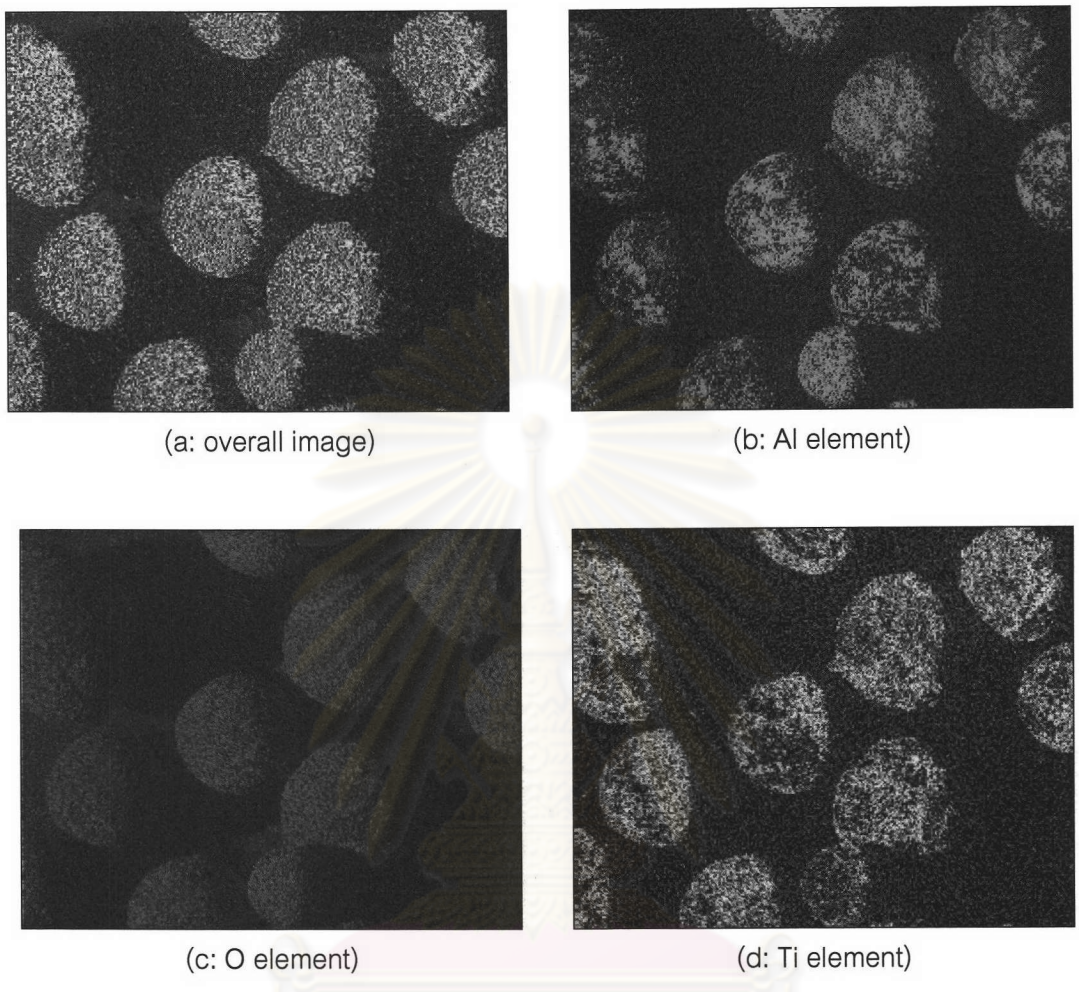

(a: overall image) (b: Al element)

(c: O element) (d: Ti element)

Figure 4.32 SEM images of TiO_2 sol (Sol_2C) coated on Al_2O_3 bead for 5 times and calcined at 400°C for 4 h; (a) overall image, (b) Al element, (c) O element and (d) Ti element

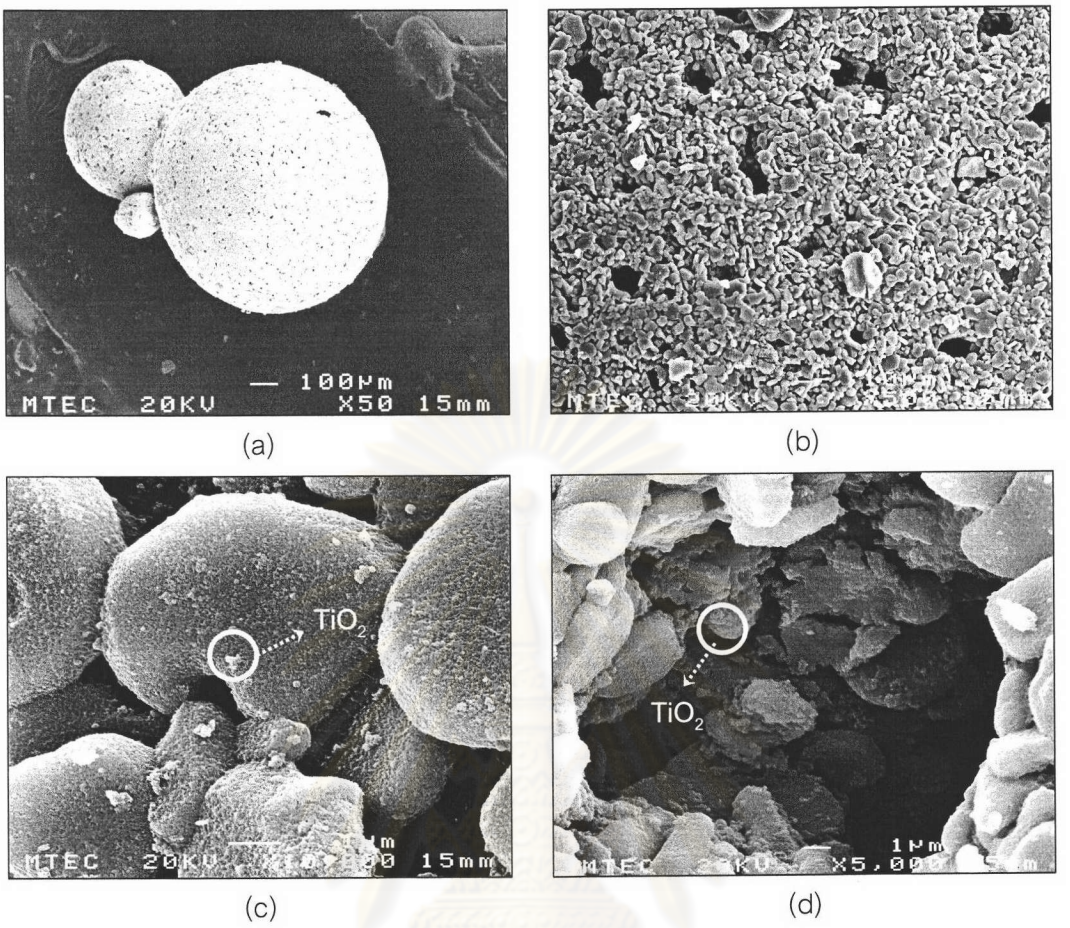

Figure 4.33 SEM images of TiO_2 sol (Sol_2C) coated on Al_2O_3 bead, calcined at 400°C for 4 h

Table 4.5 The concentration of TiO_2 calculated from XRF measurement at various numbers of coating times (1, 3, 5 and soaking for 7 days) and calcined at 400°C for 4 h

Cycle of coating	TiO_2 contents (%)
1	1.2
3	3.5
5	5.3
Soaking for 7 days	5.8

4.2.2 TiO_2 coating on glass tubes

As mentioned previously, the coating time (cycle) was a variable factor affecting the uniformity of TiO_2 coating on the substrates. Figure 4.34 shows pictures of TiO_2 coating on glass tubes for 1, 4, 8 and 12 cycles calcined at 400°C for 4 h. A thick layer of TiO_2 film was gradually grown up relatively to the increasing of coating cycles. The coating was more uniform upon increasing coating cycle. By varying the coating time, the photocatalytic determination was performed to identify the optimum condition for a good TiO_2 coating.

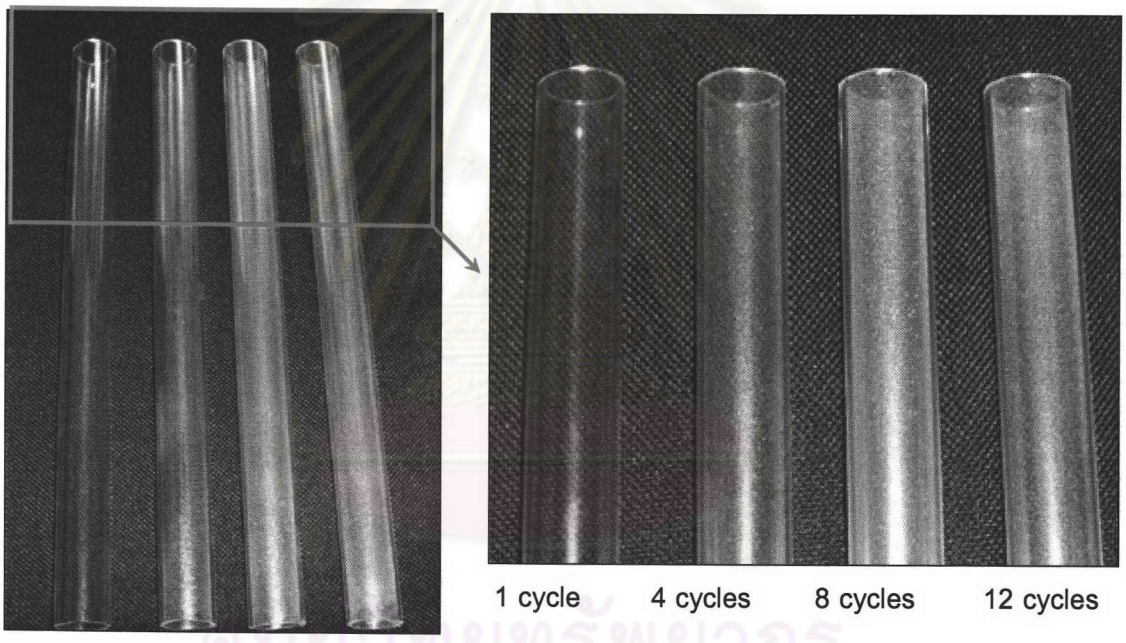

Figure 4.34 Photographs of TiO_2 coating on glass tubes for 1, 4, 8 and 12 cycles and then calcined at 400°C for 4 h

4.3 Photocatalytic efficiency determination

4.3.1 Pure TiO_2

For photocatalytic determination, the complete surface adsorption of Cibracron red (CR) on TiO_2 surface was ensured by well stirring the TiO_2 powders in a CR solution for a sufficient time. The color of the CR solution became lighter as the CR adsorbed on the TiO_2 surface. Complete adsorption was determined as the maximum absorption at 600 – 664 nm remained constant, regardless of increased stirring time.

Figure 4.35 shows the results of CR removal as the CR - adsorbed TiO_2 powders were exposed to the UV light for various times. A couple of points can be drawn from this result. Firstly, the samples containing pure anatase (Sol_2D calcined at 300 and 400°C, 4h) were the most photocatalytically reactive. However, the sample obtained from Sol_2D calcined at 300°C, 4 h also shows pure anatase phase but resulted in lower photocatalytic activity than that of the sample calcined at 400°C. It was suggested that the presence of an amorphous phase, as well as organic residue, in the 300°C-calcined powders could lower the effectiveness of a CR adsorption on the TiO_2 particles. The amorphous TiO_2 is known to have very low photocatalytic efficiency compared to that of anatase or rutile phases due to an increase in electron-hole recombination rate [34]. The activity of the samples containing mixed phase decreased with the increase of rutile phase. For instance, sample obtained from Sol_2D calcined at 500°C had a mixed anatase and rutile phase (90: 10) showed a greater photoactivity than Sol_2D calcined at 600°C, 4 h (A: R = 65: 35). Furthermore, a sample containing pure rutile phase showed the lowest photoactive. Secondly, the photoactivities of these synthesized samples were relatively low compared to that of the P-25, which consisted of 80 %wt anatase and 20 %wt rutile, and possessed surface area of 50 m^2/g. The reason of the less active in photoactivity of sample containing pure anatase phase (Sol_2D calcined at 400°C) compare to P-25 is probably due to the effect of very fine crystallite size and impurity at the surface. The sample calcined at 400°C (6.4 nm)

possessed smaller crystallite size than P-25 (d_A = 23 nm, d_R = 31.0 nm). These results were clearly compared in Figure 4.35.

The TiO_2 sample obtained from Sol_2C was also tested for photocatalytic activity. The result is shown in Figure 4.36. The photoactivity was found to show similar trend to the sample obtained from Sol_2D. That is, mixed anatase and rutile phase exhibited higher photoactivity than pure rutile phase.

For the TiO_2 powders prepared in the current work, pure anatase possessing very fine crystal size and large specific surface area was found to be most photoactive. Mixture of anatase and rutile phases was less active, while pure rutile was the least active. The photocatalytic results of these samples were different from that of the P-25, which contained mixed phase.

It is worth mentioning that calcination at various temperatures not only altered phase composition, but also altered other physical properties of the TiO_2 powders, such as crystallite size, degree of crystallinity and surface area. All of these physical properties contributed to the catalytic performance. Although anatase was believed to be more photocatalytic than the rutile phase, optimum combination of surface area which usually relates to the crystallite size, cleanness of the crystal's surface and degree of crystallinity would also attribute to the best photoactivity.

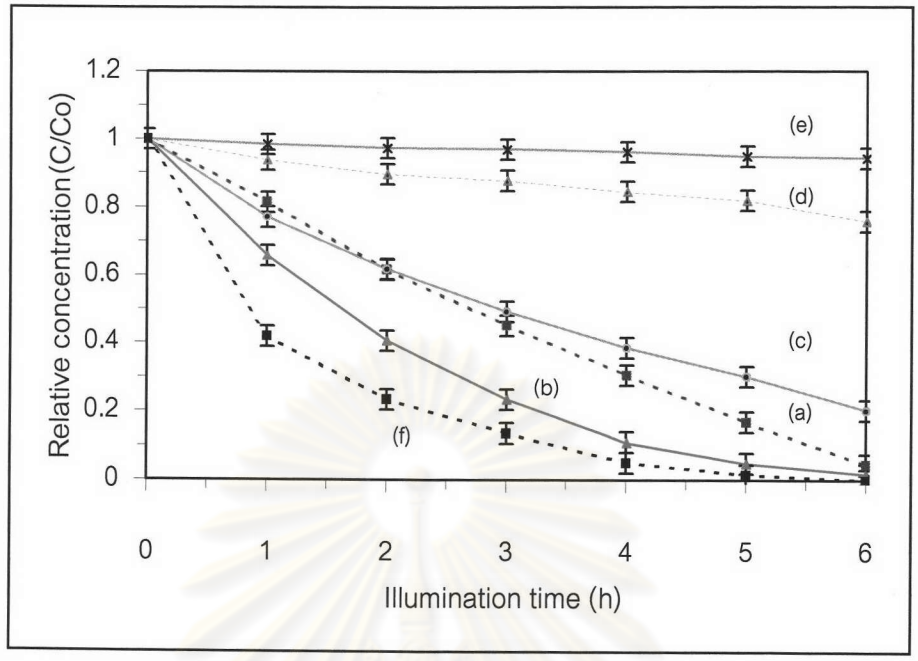

Figure 4.35 The photoremoval of Cibacron red with pure TiO_2 obtained from Sol_2D calcined at different temperatures for 4 h as a function of illumination time; (a) 300°C, (b) 400°C, (c) 500°C, (d) 600°C, (e) 700°C, (f) P-25

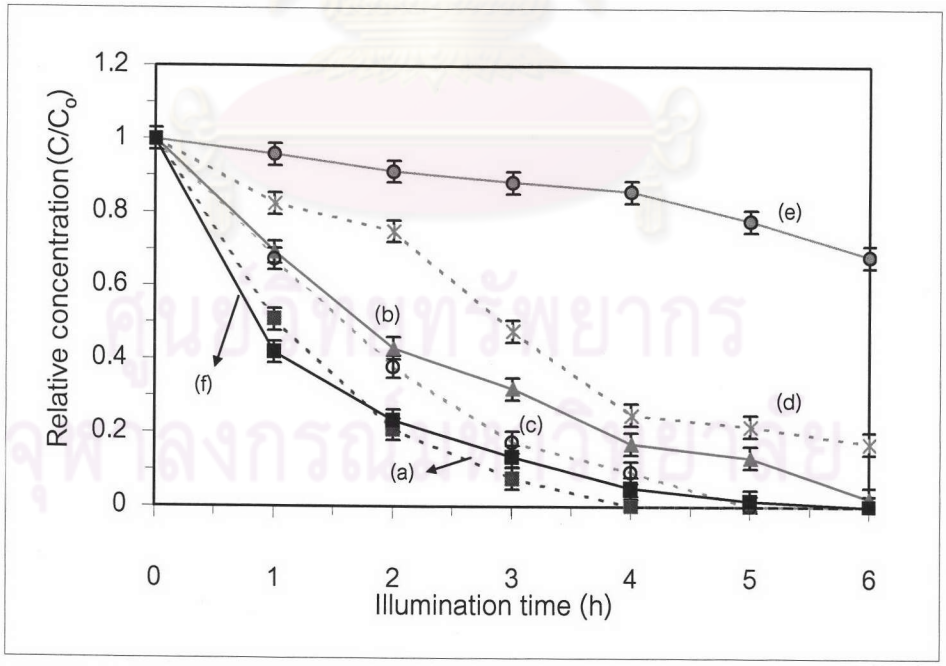

Figure 4.36 The photoremoval of Cibacron red with pure TiO_2 obtained from Sol_2C calcined at different temperatures for 4 h as a function of illumination time; (a) 300°C, (b) 400°C, (c) 500°C, (d) 600°C, (e) 700°C, (f) P-25

4.3.2 V-doped TiO_2

As described previously that the addition of V dopant retarded the anatase-to-rutile transformation. If considering only the phase composition, the TiO_2 containing high V content would be expected to exhibit high photoactivity since it consisted of mostly anatase phase. Figure 4.37 shows the photoremoval of CR by using the V-doped TiO_2 catalyst obtained from the Sol_2D (H_2O: EtOH: HNO_3 = 10:10:5) as a function of illumination time. For pure and 0.01-0.1 % of V-doped TiO_2, they were calcined at 400°C for 4 h, while the samples having 0.5-10.0% of V doping were calcined at 500°C. The result obtained from pure TiO_2 was also included for comparison. It is evident from the graph that by adding V dopant, photoactivity of the TiO_2 was not improved. It was less active than pure TiO_2. The efficiency of the TiO_2 was strongly deteriorated when the amount of V loading was higher than 0.1 %wt. It is not clear at this point about the actual role of V on photoactivity, and is the subject for further study. However, this result was similar to the study of Sene et. al. who reported the reduced photoactivity upon increasing V dopant [44]. They found that the vanadium was present in the form V_2O_5, particularly at high V loading. The vanadium in oxide form did not affect the band gap energy of the TiO_2.

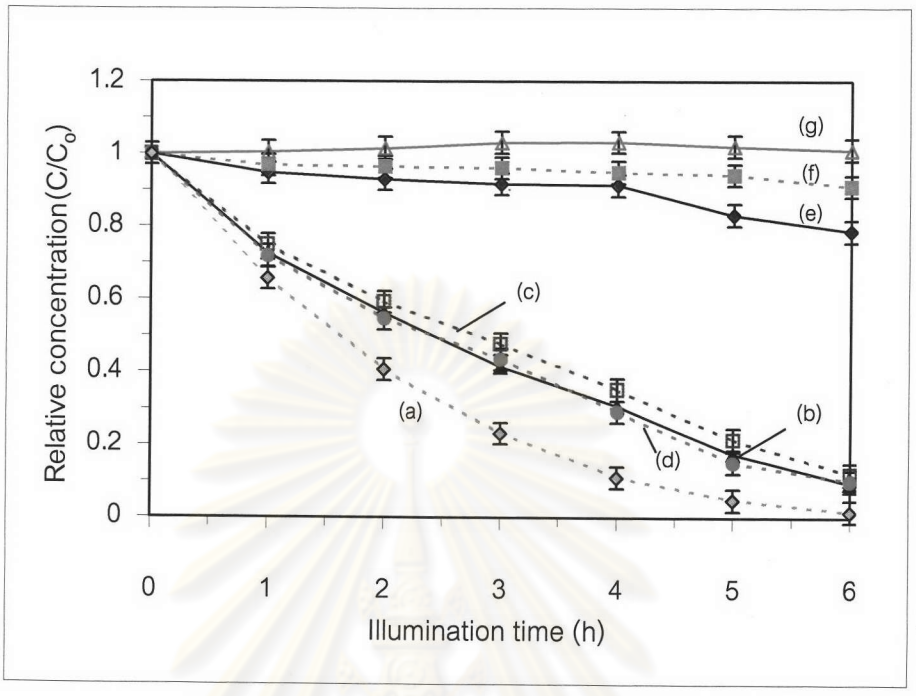

Figure 4.37 The photoremoval of Cibraconred with V-doped TiO_2 obtained from Sol_2D (H_2O: EtOH: HNO_3 = 10:10:5) calcined at 400°C (for samples (a-d)) and 500°C (for samples (e-g)) for 4 h as a function of illumination times; (a) pure TiO_2, (b) 0.01%, (c) 0.05%, (d) 0.10%, (e) 0.5%V, (f) 1.0%V, (g) 10.0%V

4.3.3 TiO_2 coating on Al_2O_3 beads

Figure 4.38 shows the removal of CR with TiO_2 coating on Al_2O_3 obtained from Sol_2C calcined at 400°C for 4 h as a function of illumination time. A 1.72 g of TiO_2-coated Al_2O_3 beads having 0.1 g of TiO_2 loading was used. The amount of TiO_2 content coated on Al_2O_3 beads is the same amount as that using in the form of powder. It was found that photocatalytic efficiency of TiO_2-coated Al_2O_3 beads was lower than that of the TiO_2 powder. This efficiency reduction is possibly due to the blocking out of the TiO_2 particles inside the pores and at the Al_2O_3 surface by surrounding Al_2O_3 beads. Thus, the photogenerate e^--h^+ pairs in TiO_2 particles by UV light illumination were inhibited, resulting in reduced photoreaction. Note that, the coated beads were easily settled out at the bottom of the container than in the form of powder.

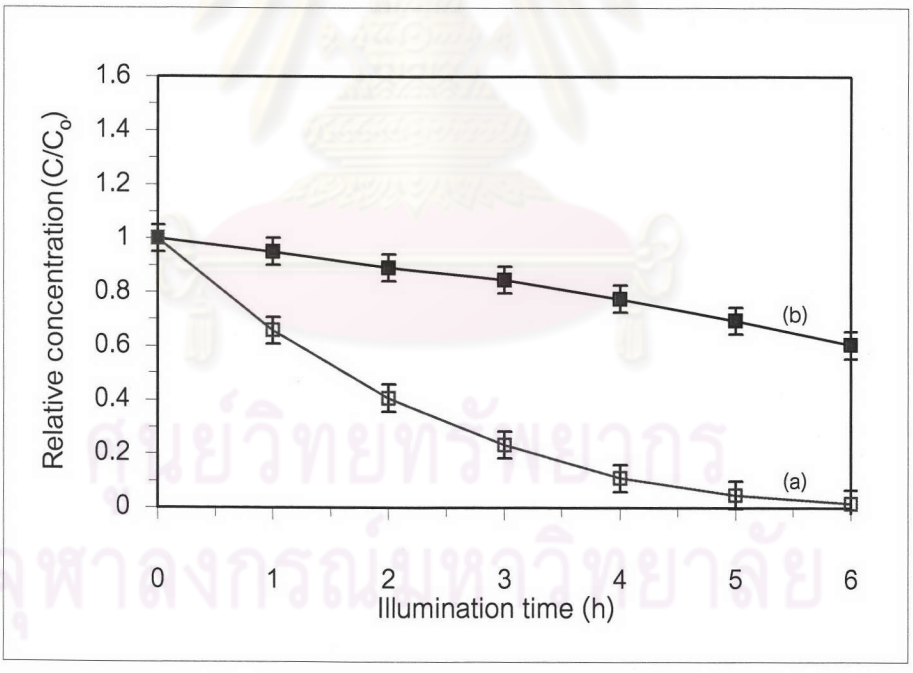

Figure 4.38 The photoremoval of Cibacron red with TiO_2 photocatalysts in the form of powders and coating obtained from Sol_2C calcined at 400°C, 4 h as a function of illumination time; (a) pure TiO_2 powders (b) TiO_2 coating on Al_2O_3

4.3.4 TiO_2 coating on glass tubes

Figure 4.39 shows the photodegradation of Methanol (CH_3OH) with TiO_2 photocatalysts immobilized on the surface of glass-tubes calcined at 400°C for 4 h as a function of coating time (1, 4, 8 and 12 cycles). As mentioned previously in chapter 3, CH_3OH in the form of gas phase was fed into TiO_2 coating on glass tube. After illumination by UV light for 8 h, the CH_3OH was decomposed to gas CO_2 and water, as shown below;

$$CH_3OH_{(g)} + 3/2O_{2\,(g)} \longrightarrow CO_2 + 2H_2O$$

The efficiency of TiO_2 coating on glass tube was improved by increasing TiO_2 loading. As seen in the figure, the yield of CO_2 was increasing from 3.39 (no catalyst) to 5.1 (12 coating cycles).

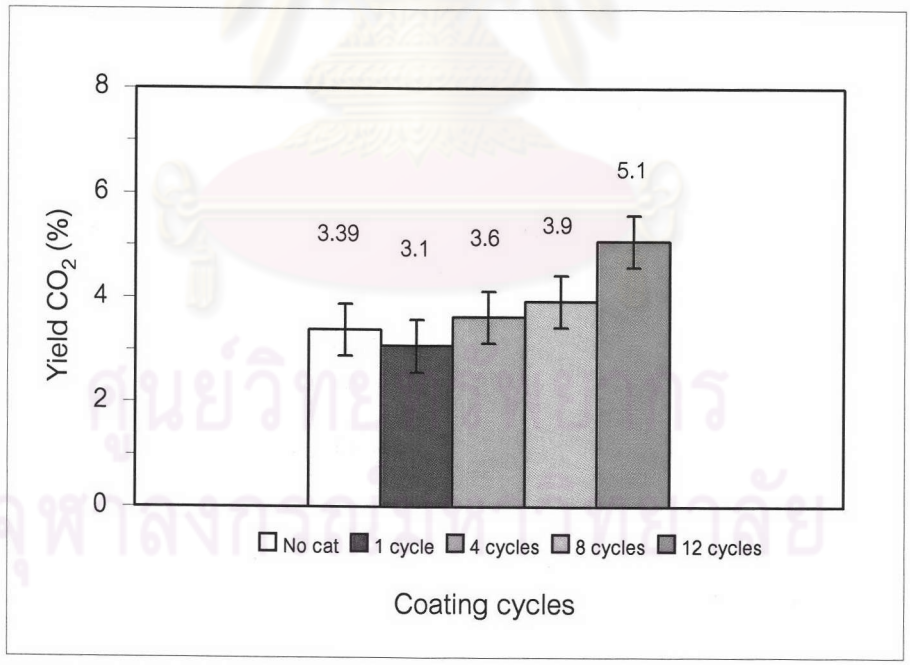

Figure 4.39 The photoremoval of Methanol (CH_3OH) with TiO_2 photocatalysts immobilized on the surface of glass-tubes calcined at 400°C for 4 h as a function of coating time; (a) No coat, (b) 1 cycle, (c) 4 cycles, (d) 8 cycles and (e) 12 cycles